Macromolecules
ARTICLE

*Macromolecules* **2010**, *43*, 7813–7827 **7813**
DOI: 10.1021/ma1010205

# Carbon Dioxide Diffusion and Plasticization in Fluorinated Polyimides

**S. Neyertz,*,† D. Brown,† S. Pandiyan,†,‡ and N. F. A. van der Vegt‡,§**

†*LMOPS-UMR CNRS 5041, University of Savoie, Bât. IUT, Savoie Technolac, 73376 Le Bourget-du-Lac Cedex, France, and* ‡*Max-Planck-Institute for Polymer Research, Ackermannweg 10, 55128 Mainz, Germany.* §*Current address: Center of Smart Interfaces, Technical University of Darmstadt, Petersenstrasse 32, 64287 Darmstadt, Germany*

*Received May 7, 2010; Revised Manuscript Received July 15, 2010*

ABSTRACT: Extensive molecular dynamics (MD) simulations of 6FDA−6FpDA, 6FDA−6FmDA, and 6FDA−DAM polyimides with $CO_2$ weight percentages up to ∼30%, were carried out to characterize the atomic level features associated with $CO_2$ diffusivity in these glassy matrices. The fluorinated polyimide models were first loaded with $CO_2$ in increments of 2% in order to mimic the experimental procedure of progressive loading and to avoid the necessity of artificially preswelling the simulation boxes. The sorption phase was then followed by a progressive desorption phase in decrements of 2%. This work covered nominal $CO_2$ concentrations up to ∼200 $cm^3$(STP) $cm^{-3}$ and amounted to a total of more than 80 simulations of 5000 ps each at 308 K, as well as an additional 20 simulations at higher temperatures. In all cases, $CO_2$ trajectories display the basic hopping-type mechanism, i.e. a combination of oscillations within available free volumes in the polymer matrix associated with occasional jumps from one site to another. There are no long-lived interactions with either the polymer or with the other penetrants, and thus, $CO_2$ is a very mobile penetrant free to access any part of the matrix free-volume. Diffusion coefficients, $D_{CO_2}$, at 308 K were estimated from a novel trajectory-extending kinetic Monte Carlo (TEKMC) method, which, based on the actual $CO_2$ trajectories during the MD production runs, allowed us to extend them by more than 3 orders of magnitude. These estimates of $D_{CO_2}$ compare very well with those obtained by a high-temperature Arrhenius extrapolation approach and with experimental evidence. Activation energies for diffusion are also validated by experimental data. All three polyimide models are able to reproduce both experimental penetrant-induced plasticization and sorption−desorption hysteresis during the few nanoseconds time scale available to MD simulations. The $D_{CO_2}$ are found to be very closely linked to the volume swelling−contraction behavior. They tend to remain low up to the start of plasticization and to be directly correlated to the gradual transition to an almost linear increase in volume at higher concentrations. The sorption−desorption hysteresis can be related to a fairly limited increase in polymer local mobility upon volume dilation, which means that the system is not able to come back to its initial structure upon desorption.

## 1. Introduction

The transport of gases through dense polymer membranes is generally described by the so-called solution-diffusion mechanism.[1−5] Gas molecules contained in an upstream compartment enter the polymer matrix, diffuse across it and desorb onto a downstream gas compartment. The rate of transport for the penetrant through the membrane is referred to as its permeability $P$, which is obtained from the gas flux normalized with respect to the membrane thickness and the applied pressure difference. In most permeation measurements, $P$ is simply expressed as the product of an average solubility coefficient $S$ and an average diffusion coefficient $D$ (eq 1):

$$P = S \times D \tag{1}$$

In eq 1, $S$ is a thermodynamic term associated with the number of gas molecules sorbing at the surface and inside the polymer matrix, while $D$ is a kinetic parameter which characterizes the mobility of the penetrant in this specific matrix. Interestingly, high permeability coefficients can either be obtained through large $D$ values, through large $S$ values or through both these effects combined.[5] The ratio of the pure gas permeabilities of gas "A" and "B", $P_A/P_B$, defines the permselectivity $\alpha_{A/B}$ of the membrane. $\alpha_{A/B}$ can itself be broken into two parts, i.e., the diffusivity selectivity $D_A/D_B$ multiplied by the solubility selectivity $S_A/S_B$.[6]

Fluorinated polyimides are interesting membrane materials for gas separation applications because of their good mechanical, chemical and thermal properties[7] combined with relatively high permeabilities and permselectivities. With respect to nonfluorinated polyimides, the introduction of $-C(CF_3)_2-$ groups in the polymer chain tends to reduce interchain interactions, increase the free-volume and decrease the ability of charge transfer complexes between dianhydride and diamine moieties.[8,9] This leads to greater solubilities for penetrants such as carbon dioxide $CO_2$[10] but the differences in permeabilities are thought to be mostly related to diffusivities and diffusivity selectivities.[6,9]

We have earlier carried out molecular dynamics (MD) simulations of three fluorinated polyimides in their pure state,[11] all of them based on the 4,4′-(hexafluoroisopropylidene)diphtalic dianhydride (6FDA), which are known to vary notably in their permeation properties with respect to $CO_2$.[10,12−18] These polyimides, i.e., the structural isomers 6FDA−6FpDA and 6FDA−6FmDA along with 6FDA−DAM, differ simply in the structure of their diamine. Their chemical formulas are shown in Figure 1. It should be noted that in the literature, 6FDA−6FpDA can be referred to as 6FDA−BAHF,[13] 6FDA−BAAF,[8,9] while 6FDA−DAM is sometimes called 6FDA−mTrMPD,[14] 6FDA−TMPDA[19] or 6FDA−3MPDA.[20]

*Corresponding author. E-mail: Sylvie.Neyertz@univ-savoie.fr.



Published on Web 08/20/2010

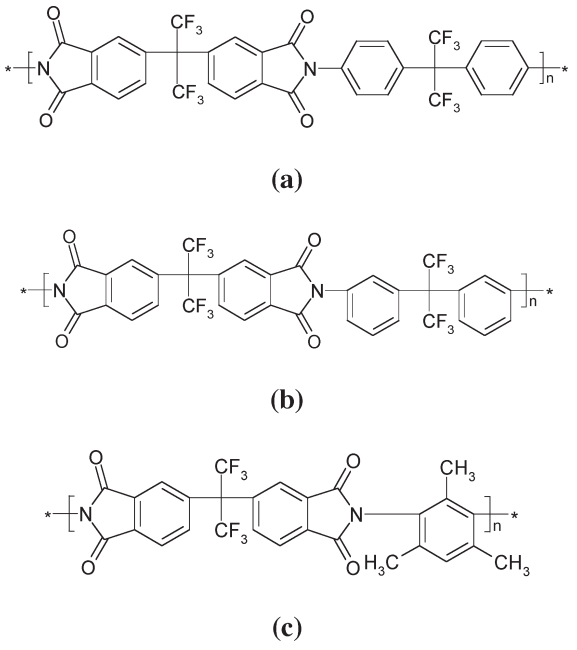


**Figure 1.** Chemical structures of (a) 6FDA−6FpDA, (b) 6FDA−6FmDA, and (c) 6FDA−DAM polyimides.

Experimentally, it has been reported that the effect of changing the bond location of the trifluoromethyl central moiety on the diamine from *para* (6FDA−6FpDA) to *meta* (6FDA−6FmDA) leads to a decrease in $CO_2$ permeability, $P_{CO_2}$, by a factor of ∼12 at near-ambiant conditions.[12,21] This was attributed by Coleman et al. to differences in diffusivities, which were of the order of ∼7.5, while solubility only varied by ∼1.6.[12] However, this could hardly be explained by the small differences in densities (1.466 for the *para*-isomer and 1.493 for the *meta*-isomer reported in that specific study),[12] intersegmental packing and fractional free volumes.[11,12] The third polyimide under study, 6FDA−DAM, is characterized by a lower density (∼1.35) and bulky nonplanar structures, which make chain packing less efficient.[11,14] Consequently, it exhibits very high $CO_2$ permeabilities and diffusion coefficients.[14] In addition to these structural considerations, it is well-known that $CO_2$ transport in glassy polymers often results in volume-swelling and plasticization of the matrix, which lead to even higher diffusivities and lower diffusivity selectivities.[22] The term "conditioning" defines the hysteretic changes in glassy polymers following exposure to such penetrants at high activities.[23,24] This is a main problem for gas separation applications as it results in enhanced transport rates of all diffusing components in mixed gas feeds and the membrane performance can be very strongly reduced.[22,25]

In addition to the work on the pure polyimides,[11] we have now carried out extensive molecular dynamics (MD) simulations of 6FDA−6FpDA, 6FDA−6FmDA, and 6FDA−DAM polyimides with $CO_2$ weight percentages ranging from 1% to ∼30%, that is covering the entire 0−60 atm pressure range. Unlike what has been done elsewhere,[26] the models were loaded progressively with $CO_2$ in increments of 2% in order to avoid the step of artificially preswelling the simulation boxes, which is clearly not very satisfactory. For each polyimide under study, the sorption phase was followed by a progressive desorption phase in decrements of 2%. This allowed us to study the conditioning effect associated with high $CO_2$ concentrations, at least on the limited time scale available to MD simulations. The different parameters associated with solubility such as the $CO_2$ sorption and desorption isotherms and the associated volume swellings and contractions have been reported elsewhere.[27] In the present paper, we concentrate rather on penetrant mobility and diffusion, which is studied here as a function of both the polymer matrix and the $CO_2$ concentration. The simulation details are given in section 2, while the penetrant trajectories and diffusivities are analyzed in section 3.

## 2. Simulation Models

All calculations were performed using the MD code of the *gmq* package[28] in its parallel form. The preparation procedures for the pure polyimide matrices[11] and for the polyimide + $CO_2$ models[27] have already been described in detail. Consequently, only their main features will be summarized here.

The parameters for the polyimides were taken from the freely available TRIPOS 5.2 force-field,[29] with the partial charges[11] being calculated using the *ab initio* Gaussian 03 code.[30] The bonds were kept rigid with the SHAKE algorithm[31] in order to use a time-step of $10^{-15}$ s in the integration algorithm. The other "bonded" interactions were described with angle-bending, torsional and out-of-plane potentials. In addition, "nonbonded" excluded-volume Lennard-Jones LJ 12−6 and electrostatic potentials were applied to all atom pairs separated by more than two bonds on the same chain or belonging to different chains. All parameters for $CO_2$ were taken from the optimized values reported by Zhang and Duan.[32] $CO_2$ is modeled here as a rigid three-site molecule with each atom carrying a partial charge and LJ 12−6 parameters. Both C−O bonds are fixed to 1.163 Å and the O−C−O angle is kept at 180°. For the latter, a special vector constraint had to be used.[33] This is very important as a flexible model for $CO_2$ will have two extra degrees of freedom, i.e. an angle bend and a rotation around the long O−C−O axis, in addition to its three translations and two rotations. The rotation around the O−C−O axis couples very poorly with the other degrees of freedom and leads to nonequipartition of the kinetic energy, an artifact which is quite visible in simulations of pure $CO_2$. As such, the O−C−O angle should remain fixed. Lorentz−Berthelot combining rules[34] were used for all unlike-atom LJ interactions and electrostatic interactions were evaluated using the Ewald summation method.[35,36] The truncation radii used for both real-space electrostatic and van der Waals contributions were set to 9 Å, and an optimal convergence of the Ewald sums[37] was obtained for ($\alpha$, $K_{max}$) parameters equal to (0.27, 13) for 6FDA−6FpDA, (0.28, 13) for 6FDA−6FmDA, and (0.28, 14) for 6FDA−DAM. Long-range corrections to the van der Waals contributions to the energy and the pressure were added using the approximation that the radial distribution functions are equal to unity beyond the cutoff.[34] The temperature $T$ was maintained at 308 K by loose-coupling to a heat bath[38] with a constant equal to 0.1 ps. The pressure $P$ was also maintained by loose-coupling with a constant equal to 5 ps.[39]

Initial configurations for the fluorinated macromolecules were obtained using the well-documented hybrid pivot Monte Carlo−molecular dynamics (PMC−MD) single-chain sampling technique.[11,40] The polymer matrices used for the diffusion studies contained three polyimide chains of length 50 monomers each, which amounted to a total of ∼10000 atoms per simulation box. The pure models were in agreement within ∼1% with the experimental densities and with available wide-angle X-ray scattering data. This is unlike the smaller packing models for 6FDA−DAM reported by Hofmann and co-workers, where their average densities differ by about 6% from the experimental data.[41] Comparative analyses of our pure matrices, including cohesive energies, Hildebrand solubility parameters, fractional free volumes, void space distributions and intermolecular as well as intramolecular interactions have all been reported elsewhere.[11] In the present work, the MD runs were carried out at 308 K (35 °C), that is above the critical temperature of $CO_2$ of ∼31 °C as in experiment,[12] and under *NPT* conditions (controlled number of atoms, controlled pressure, controlled temperature).

Gas molecules were introduced into the polymer matrices by preparing equilibrated dense boxes of $CO_2$ at approximately 1000 kg $m^{-3}$, and superimposing polyimide-containing boxes with $CO_2$ boxes of the same size. The required number of $CO_2$ (see later) was added by selecting those which overlapped least with the polymer atoms. This reduces initial high overlap energies, but in practice, this method is equivalent to a completely random insertion for mobile penetrants. To be consistent with the experimental approach and to avoid the necessity of artificially preswelling[26,41] the polyimide-containing systems, $CO_2$ loading was carried out in a progressive way. Pure polyimide samples were initially loaded with an amount of $CO_2$ corresponding to ~1% in mass of the pure polymers. *NPT* simulations were run for 500 ps, which was found to be enough for the box volume to settle, and a further 2% by mass of $CO_2$ was subsequently added to the systems to obtain 3% $CO_2$ simulation boxes. This procedure of adding 2% by mass was continued up at least until 25% of $CO_2$ had been added. Thirteen simulations boxes with increasing percentages of $CO_2$ (1% to 25% in increments of 2%) were thus obtained for the 6FDA−6FpDA + $CO_2$ and 6FDA−6FmDA + $CO_2$ systems. In the case of 6FDA−DAM + $CO_2$, the loading was extended up to 31% in order to attain a $CO_2$ concentration corresponding to a pressure of ~60 bar,[27] which has been used experimentally for conditioning of fluorinated polyimides.[23] This amounted to 16 simulation boxes for the latter, and a total of 42, corresponding to sorption for the three polyimides. As hysteresis has been reported upon desorption following conditioning of the samples,[23,24] removal of $CO_2$ starting from the highest concentrations was carried out in decrements of 2% in the same progressive way as that described above for sorption. At the end of the desorption phase, systems were also run with 0% $CO_2$ to assess the effect of conditioning on the volume of the pure polymer. This desorption procedure thus added 42 more systems to the study at 308 K. As simulations at all $CO_2$ concentrations were run for at least 5500 ps, only systems based on one pure matrix for each polyimide were used for these diffusion studies. This is unlike our work on the pure matrices[11] and on $CO_2$ solubility in these systems,[27] where results were averaged over several systems for each polyimide and for each $CO_2$ percentage. Some specific values such as the volume changes and pressures reported in the present paper will thus differ slightly from the averaged values reported in the previous papers.[11,27] In addition, 20 additional simulations were carried out at higher temperatures than 308 K in order to study the temperature dependence of diffusivity.

The true $CO_2$ concentration $C(CO_2)$ corresponding to a specific number of gas molecules $n_{gas}$ in a given polymer is simply the ratio between the volume of the gas, $V_{gas}$, and that of the penetrant-containing polymer, $V_{pol}$. $C(CO_2)$ expressed in $cm^3$ (STP)/($cm^3$ polymer), a unit which is usually written as $cm^3$ (STP) $cm^{-3}$, is given by eq 2:

$$C(CO_2) = \frac{V_{gas}^{STP}}{V_{pol}} = \frac{n_{gas} k_B T^{STP}}{P^{STP} V_{pol}} \quad (2)$$

where $V_{gas}^{STP}$ is the volume of the ideal gas at standard temperature and pressure conditions ($T^{STP}$ = 273.15 K; $P^{STP}$ = 1.013 bar), and $k_B$ is the Boltzmann constant. However, the usual experimental practice is to express the concentration with respect to the volume of the pure polymer $V_{pol\text{-}pure}$ rather than that of the penetrant-containing polymer $V_{pol}$ which is rather difficult to measure upon sorption.[23] This nominal concentration, referred hereafter as $C_0(CO_2)$, can be obtained using eq 3:

$$C_0(CO_2) = \frac{V_{gas}^{STP}}{V_{pol\text{-}pure}} = \frac{n_{gas} k_B T^{STP}}{P^{STP} V_{pol\text{-}pure}} \quad (3)$$

**Table 1. Number of $CO_2$ Molecules ($n_{gas}$) Inserted into the Polymer Systems, Approximate Mass Percentages (Obtained from the Ratio between the Mass of $CO_2$ and the Mass of the Polymer), and Nominal Concentrations $C_0(CO_2)$ Calculated Using eq 3[a]**

| | 6FDA−6FpDA | | 6FDA−6FmDA | | 6FDA−DAM | |
|---|---|---|---|---|---|---|
| % $CO_2$ | $n_{gas}$ | $C_0(CO_2)$ | $n_{gas}$ | $C_0(CO_2)$ | $n_{gas}$ | $C_0(CO_2)$ |
| 1 | 25 | 7 | 25 | 8 | 19 | 7 |
| 3 | 76 | 23 | 76 | 23 | 57 | 20 |
| 5 | 127 | 38 | 127 | 39 | 95 | 34 |
| 7 | 177 | 53 | 177 | 54 | 133 | 47 |
| 9 | 228 | 68 | 228 | 70 | 171 | 61 |
| 11 | 278 | 83 | 278 | 85 | 209 | 74 |
| 13 | 329 | 98 | 329 | 100 | 247 | 88 |
| 15 | 380 | 114 | 380 | 116 | 285 | 101 |
| 17 | 430 | 129 | 430 | 131 | 323 | 115 |
| 19 | 481 | 144 | 481 | 147 | 361 | 128 |
| 21 | 531 | 159 | 531 | 162 | 399 | 142 |
| 23 | 582 | 174 | 582 | 178 | 437 | 155 |
| 25 | 633 | 189 | 633 | 193 | 475 | 169 |
| 27 | | | | | 513 | 182 |
| 29 | | | | | 551 | 196 |
| 31 | | | | | 589 | 209 |

[a] The latter are expressed in $cm^3$ (STP)/($cm^3$ polymer), also referred to as $cm^3$ (STP) $cm^{-3}$. The number of atoms of the pure polymers are 9906 for 6FDA−6FpDA and 6FDA−6FmDA, and 8406 for 6FDA−DAM.

It is clear that $C_0(CO_2) = C(CO_2)$ if the polymer does not undergo any swelling upon sorption, which is the case for low loadings. They will only be different if the volume changes, and in the systems under study, a maximum difference of 15% between $C(CO_2)$ and $C_0(CO_2)$ was found at the highest percentages.[27] These concentrations are also related to a vapor pressure $P_{CO_2}$, which has to be applied experimentally to maintain this amount of gas in the polymer. In the models under study, $P_{CO_2}$ has been established using an iterative procedure[42] and extensive details are reported elsewhere.[27] The number of $CO_2$ molecules $n_{gas}$ inserted into the polymer as well as the corresponding mass percentages and nominal concentrations $C_0(CO_2)$ are given in Table 1 for all systems under study.

Two schematic representations of the 6FDA−6FpDA system containing 15% $CO_2$, which is the loading closest to $P_{CO_2}$ ~10 bar (*i.e.*, the pressure at which most permeation experiments are carried out)[12,13] are displayed in Figure 2 using the VMD 1.8.2 visualization software.[43] Figure 2a shows the entire simulation box at time $t$ = 5000 ps with the unfolded coordinates for the polyimide and the folded ones for $CO_2$, while Figure 2b gives a close-up of Figure 2a with all coordinates folded back into the primary box. Periodic boundary conditions were applied in the three dimensions in order to remove edge-effects.

The complexity of such systems is well illustrated by Figure 2, where the polyimide is displayed with bonds only and the penetrants with spheres. Over the course of the simulations, configurations were stored every 10 ps, the first 500 ps of each run were discarded and all analyses were carried out on production intervals of at least 5000 ps.

## 3. $CO_2$ Diffusivity in Fluorinated Polyimides

The main purpose of this work is to study the different parameters associated with $CO_2$ diffusivity in three 6FDA-based polyimides as a function of the progressive $CO_2$ loading, both upon sorption and desorption. It should be noted that no evidence of crystallinity has been reported experimentally for these materials,[21,44] so the amorphous polyimide matrices[11] should be consistent with the real systems.

**3.1. $CO_2$ Trajectories.** The mechanisms underlying small gas motion in glassy dense matrices are known to be based on combinations of oscillations within available free volumes and occasional jumping events.[45−47] Diffusion proceeds by

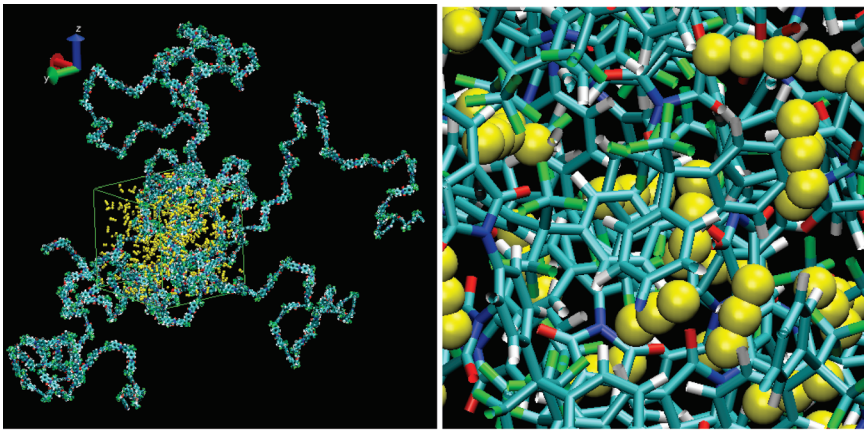

(a) (b)

**Figure 2.** 6FDA−6FpDA system loaded with 15% $CO_2$ at $t$ = 5000 ps. (a) The entire simulation box of size ~50 Å$^3$ and (b) a 13 × 13 Å$^2$ close-up of part a. The color code is the following: cyan = polyimide C, red = polyimide O, blue = polyimide N, white = polyimide H, green = polyimide F, and yellow = penetrant $CO_2$ molecules. These schematic representations are displayed using the VMD 1.8.2 software.[43]

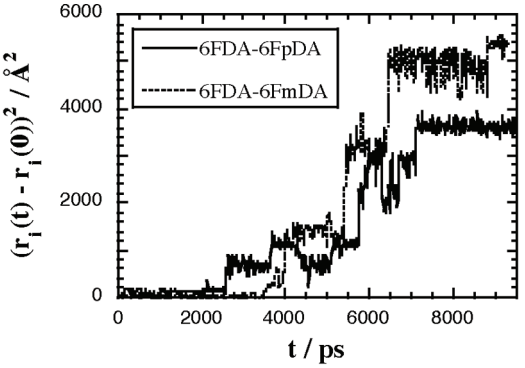


(a)

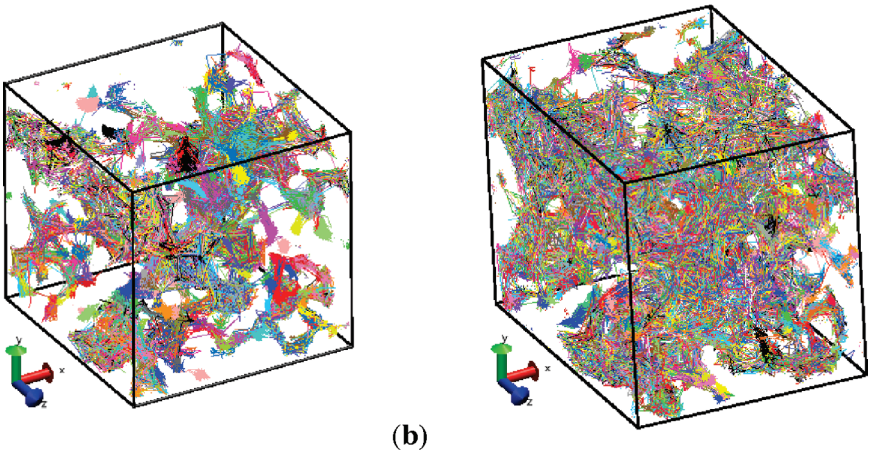

(b)

**Figure 3.** (a) Individual displacements of $CO_2$ molecules belonging either to the 6FDA−6FpDA or to the 6FDA−6FmDA systems, both loaded with 1% $CO_2$ (b) Schematic representations of $CO_2$ trajectories over 5000 ps displayed using VMD in the 6FDA−DAM systems loaded with 15% (left), box length ≈ 47.8 Å) and 31% (right, box length ≈ 49.9 Å) $CO_2$. Separate colors are used to trace the trajectories of different $CO_2$ molecules. The configurations were stored at 10 ps intervals so each straight segment of the trajectory corresponds to this time interval.

hopping between different voids, which is made possible by the temporary opening of channels within the polymer matrix.[45,46,48] The behavior of $CO_2$ in the three polyimides under study is indeed found to be similar to that of smaller and less-soluble penetrants.[40,49−51] Figure 3a displays some individual square displacements, $(r_i(t) - r_i(0))^2$, for $CO_2$ molecules belonging to the 6FDA−6FpDA and 6FDA−6FmDA 1% systems ($C_0(CO_2) \approx 8$ cm$^3$ (STP) cm$^{-3}$), which were run up to 10000 ps. In Figure 3b, the actual trajectories of the $CO_2$ carbons through the primary MD cell in the 6FDA−DAM systems at 15% and 31% ($C_0(CO_2) \approx 100$ and 200 cm$^3$ (STP) cm$^{-3}$) are visualized using VMD.

The jump mechanism is well visible in Figure 3a. Even if the individual molecules can oscillate within the same site for typically several hundred picoseconds with an amplitude of about 0−3 Å, they also jump back and forth between different sites. They occasionally get temporarily "trapped" in a dead-end but always eventually reach a position which

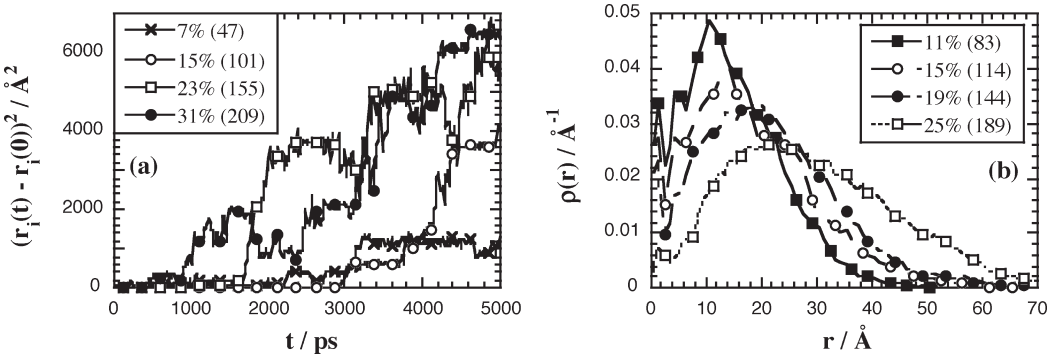


**Figure 4.** (a) Individual displacements of $CO_2$ molecules in 6FDA−DAM with different $CO_2$ loadings (b) Normalized distributions of the magnitudes $r$ of the displacement vectors over a time-interval of 4000 ps in 6FDA−6FpDA with different $CO_2$ loadings. The $\rho(r)$ have been averaged over all time-origins and over all gas molecules. The figures in parentheses in the legends are the nominal concentrations $C_0(CO_2)$ in cm$^3$ (STP) cm$^{-3}$.

allows them to take another path. It should be noted that, because of its extended $x$-axis scale, Figure 3a might give the impression that some penetrants are able to jump several nanometers in one attempt. In reality, the maximum jump distance found between two configurations (separated by 10 ps) is ∼11 Å. In addition, if one defines arbitrarily a jump as being a displacement >4 Å over 10 ps, the average jump length is found to be ∼5−6 Å in both 6FDA−6FpDA and 6FDA−6FmDA. The "larger" jumps displayed in Figure 3a thus result from a succession of small jumps over tens of ps. Close examinations of individual trajectories (Figure 3b with different colors for different penetrants) reveal that the behavior pattern can differ a lot between the penetrants in terms of time-of-residences and jump efficiencies, which is very representative of the heterogeneity of microvoids in such glassy polymer matrices. From Figure 3b, it also appears that diffusivity is reasonably isotropic in our bulk polymer models.

A closer inspection of the trajectories reveals that the different $CO_2$ molecules often have a tendency to go through the same regions of space. Although the localization of the volume accessible to the penetrants at any one instant varies as a function of time depending on the natural fluctuations of the polymer matrix, some correlations clearly persist on the MD time scale. As such, there are regions from which the penetrants are excluded and "channels" through the system that form an interconnecting and percolating network. We will take advantage of this observation later (section 3.2) in order to artificially extend the penetrant trajectories using a kinetic Monte Carlo approach. Nevertheless a clear distinction has to be made between the accessible space available at any one instant in time, i.e. typically ∼1% in terms of probe-accessible volume (PAV) for a virtual probe of radius 1.8 Å in the 15% 6FDA−6FpDA−$CO_2$ system using a simple geometric technique, similar to various other phantom sphere approaches,[27,52,53] and the cumulative total space accessed over a certain period of time (Figure 3b). Higher $CO_2$ concentrations lead to volume swelling, and as such, there is an increase in the volume accessible to the penetrants at any particular instant; i.e., the corresponding PAV is found to be ∼4% at the highest $CO_2$ contents for 6FDA−6FpDA.[27] However, as we will see in section 3.2, higher $CO_2$ concentrations are also associated with larger fluctuations in the positions of the polymer atoms. These combined effects result in the obvious increase in the cumulative total space accessed within 5000 ps in the right-hand plot of Figure 3b compared to that in the left-hand plot.

In our models, the effective volume dilation starts above a nominal concentration of ∼40 cm$^3$(STP) cm$^{-3}$,[27] which corresponds to ∼5−7% $CO_2$ depending on the polyimide under study and remains quite limited up to 80 cm$^3$(STP) cm$^{-3}$ (∼11−13% $CO_2$ and a volume swelling of ∼3%). This $CO_2$ concentration range can thus be considered as the start of plasticization, although it is well-known experimentally that it is difficult to give an unambiguous definition of this phenomenon, and that the actual technique used to observe plasticization must be explicitly stated.[22,54] Despite volume dilation, the basic jump mechanism is still found to be present at higher $CO_2$ loading. This is shown by Figure 4a, where several $CO_2$ trajectories were extracted from some 5000 ps 6FDA−DAM simulations under different loading conditions. Molecules diffuse a lot faster in the more concentrated systems (with a maximum volume swelling of 19% for 6FDA−DAM);[27] i.e., their time-of-residences are shorter and the jumps are more frequent. Interestingly, the amplitudes of the individual jumps remain fairly similar. Indeed, if a jump is again defined as being a displacement of >4 Å over 10 ps, the average jump lengths in Figure 4a are ∼4.4, 5.1, 5.3, and 5.2 Å in the order of increasing $CO_2$ concentrations. It should also be noted that the trajectories do not yet really display the very smooth paths characteristic of liquid-like diffusion. This suggests that we are still in a transition stage between the hopping-type and the liquid-like regimes, and that plasticization in the experimental pressure range is not likely to result readily in a change of mechanism for $CO_2$ motion. Figure 4b gives the distributions for the magnitudes $r$ of the $CO_2$ displacement vectors as a function of $CO_2$ loading in 6FDA−6FpDA. These distributions have been averaged over all time-origins and over all gas molecules for a time-interval of 4000 ps. In Figure 4b, the characteristic shoulder pattern of the van Hove correlation functions in the non-Fickian regime is still visible.[49] There is a weak peak at very low distances which is associated with the $CO_2$ molecules which remain, or return to, the near vicinity of their position at the time-origin, while the larger peak is related to those molecules which manage escaping from their initial environment. As $CO_2$ loading increases, the first peak tends to disappear in favor of the second diffusive one, a behavior which is fully consistent with the trajectories displayed in Figure 4a. However, even if the first peak is very attenuated, it is still present at the highest concentrations.

Specific intermolecular radial distribution functions $g(r)$ were calculated in order to characterize the possible interactions sites for $CO_2$ on the fluorinated polyimides. Some selected $g(r)$ are displayed in Figure 5. The penetrants are principally found in the vicinity of protruding chemical groups on the polymer, i.e. the 6FDA carbonyl oxygen $O_{carb}$, the $C(CF_3)_2$ fluorines on 6FDA, 6FpDA and 6FmDA as well as the $CH_3$ hydrogens on the DAM diamine. The carbonyl oxygen in polyimides has already been shown to be a

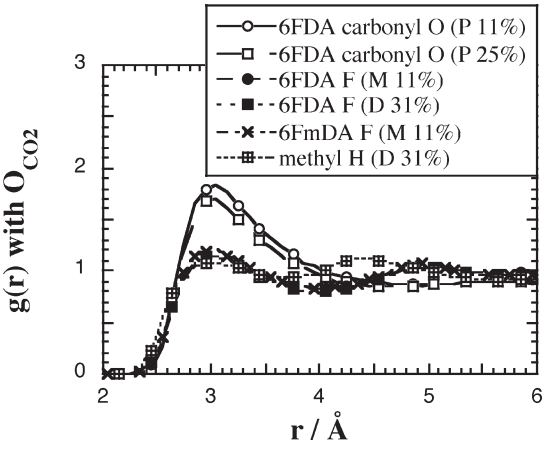


**Figure 5.** Selected intermolecular radial distribution functions $g(r)$ between the $CO_2$ oxygen, $O_{CO_2}$, and various sites on the fluorinated polymers. The letters and numbers in parentheses refer to the polyimide ($P$ = 6FDA−6FpDA, $M$ = 6FDA−6FmDA, $D$ = 6FDA−DAM) and to the $CO_2$ loading, respectively.

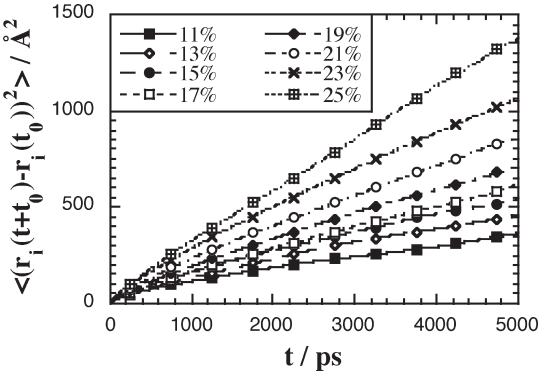


**Figure 6.** $CO_2$ mean-square displacements (MSDs) in 6FDA−6FpDA vs time plots for systems containing from 11 to 25% $CO_2$. The MSDs have been averaged over all penetrants in a system and all possible time-origins $t_0$.

preferential interaction site for $H_2O$[55] and, even if the $O_{carb}\cdots O_{CO_2}$ peaks are less well-defined than the $O_{carb}\cdots O_{water}$ ones, this is also the case for $CO_2$. It is supported by the correlation between the carbonyl oxygen in carbonate polyethers and the increased $CO_2$-philicity of such surfactants.[56] As far as the fluorines are concerned, *ab initio* molecular orbital calculations of $CO_2$ and fluorinated compounds have reported a specific quadrupole-dipole interaction between the gas and accessible F sites on the polymer matrix.[57] However, the $F\cdots O_{CO_2}$ peaks in Figure 5 are flatter than those with the carbonyl, which suggests that the $CO_2$ interactions with the fluorines are weaker than those with $O_{carb}$.

The $g(r)$ displayed in Figure 5 summarize the main features found for all three polyimides. The first point is that there is very little influence of the $CO_2$ loading. This can be seen in the $O_{carb}\cdots O_{CO_2}$ $g(r)$ (open squares and circles) which are almost superimposable, irrespective of whether the 6FDA−6FpDA system is loaded with 11% or 25% $CO_2$. The total number of penetrants around a given site on the polymer, obtained by integration of the $g(r)$, is directly proportional to the nominal concentration $C_0$. The $g(r)$ are not correlated either to the differences in the entire chemical structure, as the interactions of $CO_2$ with the 6FDA dianhydride are found to be very similar in all three systems. This is illustrated in Figure 5 by the 6FDA dianhydride $F\cdots O_{CO_2}$ $g(r)$ for 6FDA−6FmDA (filled circles) and 6FDA−DAM (filled squares). It is also superimposable with the diamine $F\cdots O_{CO_2}$ $g(r)$ (crosses), while the DAM methyl $H\cdots O_{CO_2}$ $g(r)$ is very similar. This suggests once again that $CO_2$ favors those specific groups that are easily accessible rather than forming interactions with more sheltered parts of the polymer. Since we did not find either any evidence of $CO_2\cdots CO_2$ clusters inside the polyimide matrix,[27] the overall picture that emerges is that of a penetrant which is free to access any part of the available free-volume in the polymer matrix. This agrees with the trajectories visualized in Figure 3b.

**3.2. Diffusion regimes for $CO_2$ at 308 K.** In MD simulations, diffusion coefficients are usually obtained from the penetrant mean-square displacements, MSDs $= \langle (r_i(t+t_0) - r_i(t_0))^2 \rangle$, averaged over all penetrants and all possible $t_0$ time origins of the production runs. The MSDs can then be used to evaluate the self-diffusion coefficients $D$ using Einstein's equation:

$$D = \lim_{t \longrightarrow \infty} \frac{1}{6t} \langle (r_i(t+t_0) - r_i(t_0))^2 \rangle \qquad (4)$$

However, eq 4 is only valid under the assumption that the gas molecules follow a random walk. In dense polymers, where penetrant motion is strongly restricted by the immediate environment, the random-walk condition is obtained within the framework of a long-time Fickian diffusive limit, i.e. when the MSDs are proportional to $t$. In the intervening time, with the exception of a short-time ballistic regime at the very start, the MSD curves are usually found to be proportional to $t^n$ with $n < 1$, which characterizes the so-called anomalous diffusion regime.[45,46,49,58] The actual diffusion regime can be identified from log(MSD) − log($t$) plots,[45,46] where the transition from the anomalous to the Fickian regime is characterized by a slope tending to one.[59]

The penetrant MSDs obtained during the sorption procedure of the 5000 ps production run in 6FDA−6FpDA are given in Figure 6 for the 11−25% $CO_2$ loading range. The MSDs for the lower $CO_2$ loadings in 6FDA−6FpDA (5%, 7% and 9%) are almost indistinguishable from that at 11% $CO_2$ (filled squares in Figure 6). The only exceptions are the MSDs at very low loadings which appear to be ∼1.5 times higher than the 5−11% range. However, these systems correspond to associated external pressures $P_{CO_2} < 0.2$ bar,[11] and clearly suffer from poorer statistics due to the reduced number of permeants. Indeed, similar plots (not shown) to Figure 6 are obtained for 6FDA−6FmDA and 6FDA−DAM. In the case of 6FDA−6FmDA, the only curve that is separated from the other low-loading curves is the 1% MSD, whereas for 6FDA−DAM the 1% and 3% MSDs overlap with the other low-loading curves.

The features displayed in Figure 6 are found to be qualitatively identical for all three polyimides. As mentioned above, the MSDs up to the $C_0 \sim 40-80$ cm$^3$ (STP) cm$^{-3}$ concentration range are almost indistinguishable from each other. Interestingly, this includes the experimental plasticization concentration of 6FDA−polyimides, reported as being equal to ∼57 cm$^3$ (STP) cm$^{-3}$.[60,61] On the other hand, the MSDs at higher $C_0$ keep on increasing with $CO_2$ concentration. However, it is not possible to extract true diffusion coefficients from Figure 6 as the slopes obtained from the corresponding long-time limits of the log(MSD)−log(t) plots fall within the range 0.6−0.9.

Figure 3b showed that the actual trajectories of $CO_2$ molecules are associated with regions from which the penetrants are excluded and to "channels" that form an interconnecting and percolating network through the glassy polymer matrix. While the time scale of the MD simulations is still too short for the penetrant movements to appear as random walks, it should be possible, at least in these

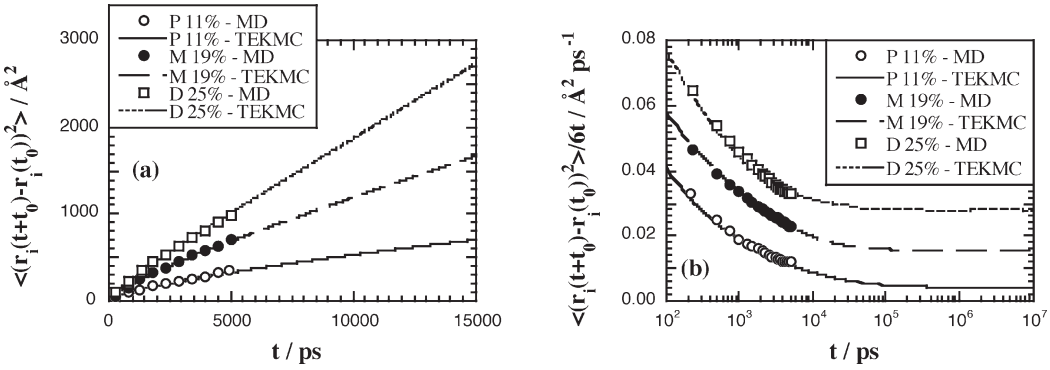


**Figure 7.** (a) $CO_2$ mean-square displacements (MSDs) as a function of time $t$ in various systems obtained either directly from the actual 5000 ps MD simulation runs ("MD", symbols) or from the Trajectory-Extending Kinetic Monte Carlo procedure ("TEKMC", lines). The letters and percentages refer to the polyimide (P = 6FDA−6FpDA, M = 6FDA−6FmDA, D = 6FDA−DAM) and to the $CO_2$ loading, respectively. The optimal subcell grid resolution was found to be 0.5 Å for P 11%, 0.65 Å for M 19% and 0.7 Å for D 25%. (b) same as (a) except that the MSD/6$t$ is displayed as a function of $t$ on an extended time scale. Note that the $x$-axis is displayed on a logarithmic scale.

intermediate to high concentration regimes, to obtain an estimation of the true diffusion coefficients (based on the assumption that these channels persist) if these trajectories within the percolating channels could be propagated further in time. In order to extend the 5000 ps time range of our MSDs curves (Figure 6), we introduce here a variant of the kinetic Monte Carlo (KMC) approach,[46,48,62−67] for which the applications in the field of low concentration (infinite dilution) polymer−penetrant systems have been extensively reviewed by Theodorou (see Chapter 2 of ref 5). Providing that the penetrant molecules are able to explore a significant part of a periodic system, i.e., that they reveal within the duration of the explicit MD simulation a sufficient amount of the interconnecting network of channels, the first phase of our procedure is to assign the actual trajectories to subcells of the primary MD box based on the penetrant positions. The resolution of the grid for the subcells is a key parameter which can be optimized (see later). For each subcell that has been visited by a penetrant molecule, the identity of all subcells that it moves to at subsequent steps is recorded, along with the number of times that such subcells are being moved to. If the penetrant remains in the same subcell over several stored configurations, this is also recorded. As a result, we obtain a probability matrix for jumps to occur between specific subcells based on the actual stored configurations of the MD production run. In a second separate kinetic Monte Carlo phase, a number of random walks are initiated from randomly selected subcells among those that have been visited. At each step of a walk, a subcell to jump to is selected with a probability corresponding to that found in the first phase from the list of subcells that can be reached from the current subcell. In order to avoid the random walks becoming trapped, the probability matrix is artificially symmetrized. This is equivalent to enforcing detailed balance, *i.e.* the flux of particles from cell I to J is the same, on average, as those from cell J to cell I. Since this technique allows us to extend the penetrant trajectories based on the actual existing runs, we refer to it as "trajectory-extending kinetic Monte Carlo" or "TEKMC".

We emphasize at this point that our TEKMC approach is based on a relatively straightforward analysis of the *actual trajectories of gas molecules in the polymer*. As mentioned above, it is thus clear that the TEKMC method is only valid in a concentration regime where enough of the percolating paths through the polymer system are revealed in the limited duration of the atomistic MD simulation. It is thus most appropriate at *intermediate to high concentrations*, which are the subject of this particular study. On the other hand, TEKMC is inappropriate in the very low concentration regime as the required percolating paths will not be revealed within a reasonable simulation time. As such, the TEKMC approach is not an alternative to the more sophisticated, and more ambitious, Gusev−Suter[46,62,63,66,67] or Greenfield−Theodorou[48,64,65] approaches that are specifically designed to obtain the diffusion coefficient of a penetrant in the infinite dilution limit from an analysis of the pure polymer system. However, as will be demonstrated here, there are regimes where brute force MD simulations are too costly to determine the limiting diffusion coefficient directly but where TEKMC can be used to make fairly reliable estimates of this property.

The application of the TEKMC technique to our polyimide + $CO_2$ models at 308 K is illustrated in Figure 7 for different matrices and $CO_2$ loadings. As stated above, the results are sensitive to the choice of the resolution of the subcell grid, which should match to some extent the natural fluctuations of a penetrant molecule between undergoing jumps to different sites. If the grid resolution is too small, the connectivity between the different trajectories taken by the penetrants will be underestimated and thus lead to slower diffusion. On the other hand, if it is too coarse, it will overestimate the connectivity and lead to faster diffusion. However, this parameter can be easily tuned in TEKMC by first reproducing the MSDs over the time-interval of the original MD runs. In the systems under study here, the subcell grid resolution was found to be typically of the order of 0.6−0.9 Å.

Figure 7 shows that TEKMC is clearly very efficient at extending the penetrant trajectories. The MSDs are correctly reproduced on the initial 5000 ps time scale of the MD productions runs (Figure 7a), which suggests that the probability matrices and the grid resolutions used are appropriate. In addition, the time scale of the random walks in TEKMC has been extended up to $10^7$ ps, *i.e.*, by more than 3 orders of magnitude (Figure 7b), at negligible costs in terms of computing time. In all systems under study, this was found to be enough to reach the long-time Fickian diffusive limit and obtain the diffusion coefficient for $CO_2$, $D_{CO_2}$, from the plateau value of the MSD/6$t$ vs $t$ curve displayed in Figure 7b (eq 4). It is interesting to note that the optimal grid resolution tends to slightly increase when the MSDs are faster, and as such, that it is truly representative of the mobility of the penetrant. Another point to reflect upon is that the results will of course be strongly dependent on the original 5000 ps

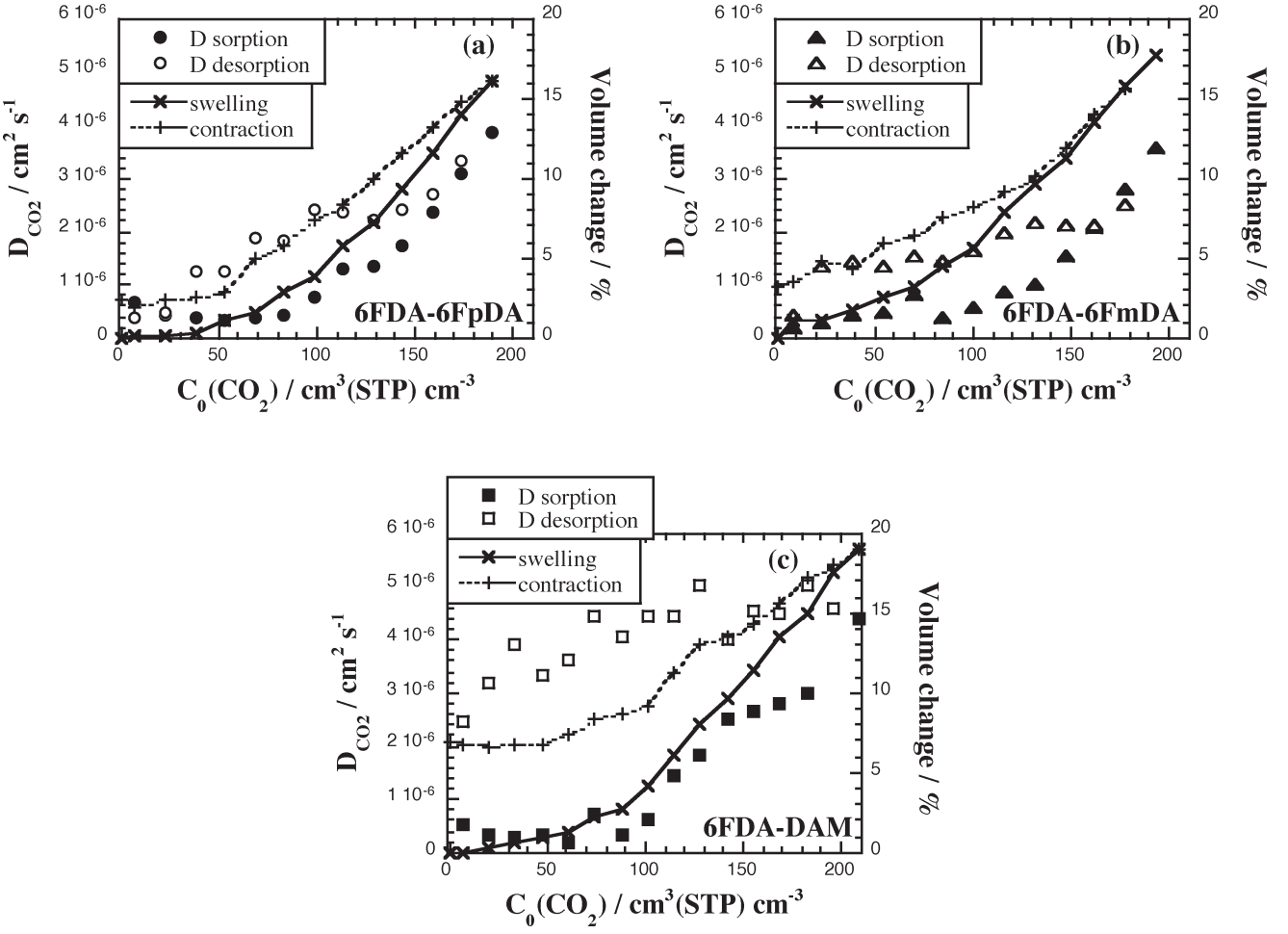


**Figure 8.** Left axis: $CO_2$ diffusion coefficients $D_{CO_2}$ in $cm^2\ s^{-1}$ as a function of the polyimide and the $CO_2$ nominal concentration. The $D_{CO_2}$ are extracted from the penetrant MSDs extended up to $10^7$ ps using the TEKMC method (see Figure 7). The filled symbols refer to $D_{CO_2}$ obtained during the progressive loading sorption phase and the open symbols to the progressive desorption phase. Right axis: the corresponding percentages of volume swelling during sorption and volume contraction during desorption (eq 5). Key: (a) 6FDA−6FpDA, circles; (b) 6FDA−6FmDA, triangles; (c) 6FDA−DAM, squares.

MSDs, which are at the basis of the probability matrix for the jumps to occur in TEKMC. The penetrants must have moved sufficiently far over the course of the MD simulation for the subcells connectivity to percolate the system. This condition can be checked by analyzing the subcell connectivity and visualizing the trajectories. In the case of $CO_2$, this is clearly the case (Figure 3b) with the exception of the very low loading systems which suffer from limited statistics. We will also show later (section 4) that the diffusion coefficients obtained directly at 308 K using TEKMC compare favorably to those obtained via a high-temperature extrapolation Arrhenius approach, in which we are actually able to reach the Einstein limit for diffusion at several temperatures ranging from 400 to 900 K within the time scale available to MD simulations. Furthermore, the TEKMC technique applied on the high-temperature systems gives the same diffusion coefficients than those obtained from the actual trajectories (results not shown). TEKMC is thus both able to reproduce the trajectories for systems which have reached the Fickian regime and predict $D_{CO_2}$ for systems where this regime is difficult to reach with MD simulations.

The values of the $CO_2$ diffusion coefficients were extracted using TEKMC for all three polyimides and all $CO_2$ loadings under study, both during the sorption and the desorption phases. They are displayed on the same scale for 6FDA−6FpDA, 6FDA−6FmDA, and 6FDA−DAM in Figure 8 as a function of the nominal $CO_2$ concentration $C_0$. The percentages of volume change defined as:

$$\text{volume change} = \frac{(V(C_0) - V_0)}{V_0} \times 100 = \frac{\Delta V}{V_0} \times 100 \quad (5)$$

where $V_0$ is the volume of the pure polymer prior to any $CO_2$ insertion and $V(C_0)$ is the volume of the simulation box corresponding to a specific loading are also indicated on the right-hand axes of Figure 8a-c.

The swelling behavior has been described in detail in the associated solubility paper.[27] When averaged over three independent samples, the behavior of the three types of polyimides is quite close, i.e., the volume increases up to 16.0 ± 0.5% for 6FDA−6FpDA, 16.2 ± 0.2% for 6FDA−6FmDA, and 18.4 ± 0.4% for 6FDA−DAM for the highest $CO_2$ concentrations under study. The slight differences between the model polymers can be attributed to the differences in their initial free-volume fractions but the limiting model partial molar volume of $CO_2$ is found to be $30 \pm 2\ cm^3\ mol^{-1}$ in all three cases. Following exposure to the highest $CO_2$ concentration, the simulation box volume decreases when $CO_2$ molecules are progressively removed, but it never returns to the values of the volume found in the sorption phase. Indeed, this conditioning eventually results in average volume increases of ~2.5%, ~4% and ~7% for

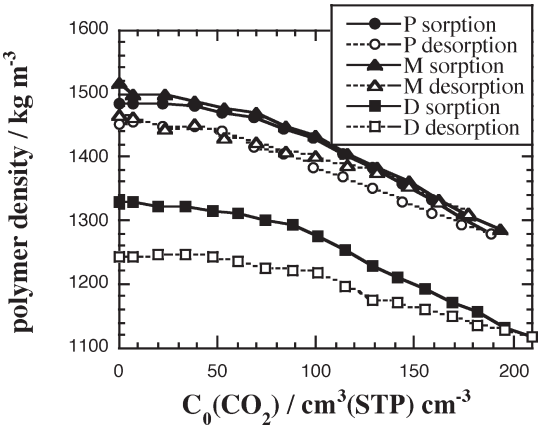


**Figure 9.** Polymer packing densities in kg $m^{-3}$ as a function of the $CO_2$ nominal concentration, both during sorption (filled symbols) and desorption (open symbols). The letters refer to the polyimide (P = 6FDA−6FpDA, M = 6FDA−6FmDA, D = 6FDA−DAM).

the pure 6FDA−6FpDA, 6FDA−6FmDA, and 6FDA−DAM polymers, respectively, when all $CO_2$ molecules have been removed.[27] The results for the individual samples shown in Figure 8 are very similar.

Penetrant-induced hysteresis, i.e. the fact that significantly higher permeability values are measured when the pressure is decreased stepwise following exposure to high-pressure $CO_2$ (when compared to a simple pressurization procedure) is a well-known process experimentally[22−24,61,68] and thus clearly occurs in glassy polymers even over the few nanoseconds time scale available to MD simulation models. It should be noted that experimental conditioning at 60 atm for 6FDA−6FpDA and 6FDA−6FmDA had to be carried out for several weeks in order to attain "steady state", i.e., a change in permeabilities of less than 0.5% per day over a 48 h period,[23,24] and that conditioning time is known to affect the permeation behavior.[69] Even though it is impossible to study with MD simulations the effects of such a long-term conditioning, the models reveal the immediate effect of exposure to high $CO_2$ concentrations in polymers. Experimentally, this is usually explained by the excess free-volume being trapped in the polymer matrix in the form of disruptions because of the relaxation time of the polymers which are much greater than the rate of penetrant removal.[23] On the basis of dilation kinetics for the sorption of $CO_2$ in some polyimide matrices, Wessling et al.[25,68] described the sorption process as the sum of contributions from "Fickian" sites referring to the voids present in the pure matrix and "relaxational" sites newly created to accommodate the high penetrant concentrations. The latter are directly linked to the morphological alterations of the matrix and are thought to be related to larger-scale motions than the Fickian sites. Because of the smaller lubrication effect for a desorption pressure step compared to a sorption pressure step, the relaxational sites are so slow to relax that the volume contraction isotherm always lie above the dilation isotherm. This interpretation[68] is coherent with our molecular models. The simulation boxes dilate above a nominal $CO_2$ concentration of ~40 $cm^3$ (STP) $cm^{-3}$, but even for the highest loadings in Table 1, this does not lead to a very significant increased mobility of the matrix, at least in the time scale of the MD simulations (see polymer MSDs in Figure 10). As such, the systems are not able to recover their initial structure and thus the excess free-volume that has been created by the swelling remains to a certain extent.

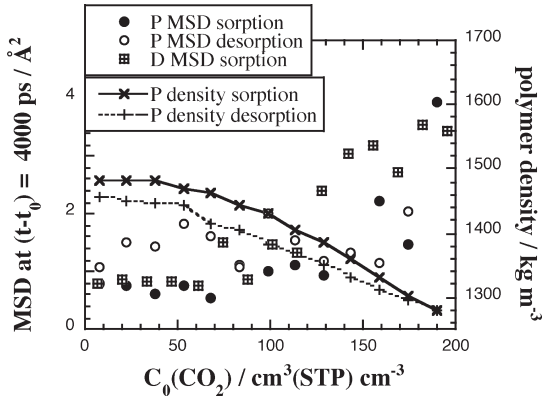


**Figure 10.** Left axis: Number-averaged MSDs values for all polymer atoms in 6FDA−6FpDA (P) and 6FDA−DAM (D) at a time-interval of 4000 ps. Averages were taken over all possible time-origins. The filled and open circles refer to the sorption and desorption phases in 6FDA−6FpDA, respectively, while the squares refer to sorption in 6FDA−DAM. Right axis: the corresponding 6FDA−6FpDA packing densities during sorption and desorption.

For the three polyimides under study, the $CO_2$ diffusion coefficients during the sorption phase (filled symbols in Figure 8) tend to remain fairly low up to $C_0(CO_2) \approx 40-80$ $cm^3$ (STP) $cm^{-3}$. As noted before, this is the start of the swelling behavior with <1% volume change at ~40 $cm^3$ (STP) $cm^{-3}$ and ~3−4% at ~80 $cm^3$ (STP) $cm^{-3}$ (Figure 8). The fact that the experimental $CO_2$ plasticization concentration for 6FDA−polyimides, ~57 $cm^3$ (STP) $cm^{-3}$, falls right in this range[60,61] is a very strong validation for our models. $CO_2$ plasticization concentrations are reported as being of the order of 40−60 $cm^3$ (STP) $cm^{-3}$ for noncross-linked polyimides,[61,70] but can also vary with processing factors such as thermal treatments.[22,70] Wind et al. found for a series of DAM-based cross-linked copolymers that the onset of plasticization can be correlated with a sorbed $CO_2$ partial volume of 29 ± 2 $cm^3$ $mol^{-1}$,[70] a value that agrees perfectly with our model partial molar volume of $CO_2$ of 30 ± 2 $cm^3$ $mol^{-1}$.[27] Working with different gases in polyimides, Visser et al. concluded from dilation isotherms that such an onset is likely to be determined simultaneously by the partial molar volume of the gas and its solubility.[25] Before the start of volume dilation, the penetrants have to be fitted into a very similar amount of free-volume, which is characteristic of the pure matrix. Within the available statistical resolution, the $D_{CO_2}$ up to $C_0(CO_2) \approx 80$ $cm^3$ (STP) $cm^{-3}$ are actually rather similar (Figure 8). This confirms that the mobility of one penetrant is unlikely to be affected by that of another penetrant, except for purely space-occupying considerations. It also agrees with the known decrease in permeability at low pressures in untreated samples, which is generally attributed to decreases in solubility rather than in diffusion coefficients.[23]

As far as the higher $C_0$ are concerned (Figure 8), the increase in $D_{CO_2}$ is directly correlated to volume swelling. Coleman and Koros[23] have studied $CO_2$ plasticization in a series of fluorinated polyimides, among which 6FDA−6FpDA and 6FDA−6FmDA, with plasticization being there defined as the increase in diffusivity of a penetrant due to the presence of other penetrants in the surrounding neighborhood. They describe the permeability as increasing significantly during the first 2 days following exposure to $CO_2$, a stage which is followed by a slow creep to the steady-state permeability over a 2−3 week period.[23] The overall increase in permeability is reported as being ~6.7 for 6FDA−6FpDA and ~7.9 for 6FDA−6FmDA at 60 atm compared to that at

10 atm in unconditioned films. In terms of diffusivity, it seems from Figure 5 in the work of Coleman and Koros[23] that the increase in $CO_2$ diffusivity would be about a factor of 14 for 6FDA−6FpDA between 10 and 64 atm, although this value falls to ∼7 if one looks at the 10 to 56 atm range. As noted above, the experimental time scales can never be directly accessed using MD simulations and we can realistically only hope to model the initial immediate stage. In Figure 8, the increase in diffusivity between 100 and 200 $cm^3$ (STP) $cm^{-3}$ is about a factor 5 for 6FDA−6FpDA and ∼6.5 for 6FDA−6FmDA, which remains fairly consistent with experimental evidence. It is slightly larger, ∼7.2, for 6FDA−DAM. In terms of model void space analyses, the probe-accessible volume, PAV, was obtained from repeated random insertions of a virtual probe of radius of 1.8 Å into the simulation boxes, by taking into account or excluding the actual $CO_2$ molecules present in the systems.[27] Before the start of volume dilation, the $CO_2$-excluded PAV hardly changed whereas the $CO_2$-included PAV gradually decreased as holes were being filled up. Above $C_0$ ∼40−50 $cm^3$ (STP) $cm^{-3}$, the $CO_2$-included PAV remained very small whereas the $CO_2$-excluded PAV reflected the same behavior as the volume swelling curve. This confirms that the volume dilation is really dependent on the number of penetrants and this was accompanied by a decrease in the percentage of small holes and an increase in the percentage of larger holes in the systems.[27] As expected, the hysteresis found in the volumetric analyses is also reflected in the diffusivities, with the $D_{CO_2}$ being quite a bit higher during desorption (open symbols in Figure 8) than during sorption (filled symbols in Figure 8). Interestingly the largest differences are seen for the low $CO_2$ loadings, i.e., in systems with an initially limited volume swelling. This agrees with the qualitative features of the conditioning loops found experimentally where permeabilities get even higher at lower loadings during the desorption phase, because of a combination of higher diffusion and solubility coefficients.[23,24] It is clearly related to the difficulty for the polymer to lose the excess free-volume created by the conditioning and redensify toward the structures of unswollen systems.

In the literature, there is a fairly large amount of scatter in experimental $D_{CO_2}$ at 308 K which can be found at low pressures (typically around 10 atm) for the three 6FDA-based polyimides.[12−18] This is not surprising considering the large number of factors that affect permeation in glassy systems,[71] such as molecular weight,[72] film thickness,[73] residual solvent,[74] heating cycle,[75,76] casting conditions[76] or aging.[77] It should also be noted that $D_{CO_2}$ is usually obtained indirectly by dividing permeability, measured using a gas permeation equipment by solubility, which is determined by a sorption cell.[12−14] Tanaka et al. estimate the uncertainties as being ±3% for $P$ and $\pm 3 \times 10^{-4}$ $cm^3$ (STP) $cm^{-3}$ $cmHg^{-1}$ for $S$.[13,14] Bos et al. report probable errors in permeabilities ranging higher, i.e. from 4% to 10%, and relative errors in sorbed $CO_2$ concentrations from ∼5% to ∼17%.[54] From Figure 8a, the model $D_{CO_2}$ for 6FDA−6FpDA at 308 K are of the order of $\sim 3-4 \times 10^{-7}$ $cm^2$ $s^{-1}$ (Figure 8a), while Coleman et al.[12,21] report $1.1 \times 10^{-7}$ $cm^2$ $s^{-1}$ and Wang et al.[18] $1.7 \times 10^{-7}$ $cm^2$ $s^{-1}$. The model agrees even better for 6FDA−DAM, where $D_{CO_2}$ is $\sim 4-6 \times 10^{-7}$ $cm^2$ $s^{-1}$ (Figure 8c) while Tanaka et al.[10,14] give $5.4 \times 10^{-7}$ $cm^2$ $s^{-1}$. On the other hand, the model appears to overestimate the diffusion coefficients for 6FDA−6FmDA, $\sim 2-3 \times 10^{-7}$ $cm^2$ $s^{-1}$ (Figure 8b), i.e. somewhat higher than the only experimental value available by Coleman et al. of $\sim 0.134 \times 10^{-7}$ $cm^2$ $s^{-1}$.[12,21] In simulations, an agreement within a factor 2−3 for the diffusion coefficient is usually considered as very good,[45] taking into account both the simplified nature of the modeling and the different experimental conditions. It is clear that 6FDA−6FpDA and 6FDA−DAM fall well within this range. In the case of 6FDA−6FmDA, the model $D_{CO_2}$ are too close to those in 6FDA−6FpDA to really agree with the permeability of $CO_2$ in the *para* isomer being ∼12 times higher than that in the *meta* isomer.[12,21]

If one compares the symmetric 6FDA−6FpDA and asymmetric 6FDA−6FmDA isomers, their density difference is known to be rather small both from an experimental and from a modeling point of view, *i.e.*, about 1%.[11] Coleman et al. did point out that, although this could reflect small variations in intersegmental packing and void spaces, such a limited difference in density is not enough to explain the respective gas transport properties.[12,21] However, the same group also reported that both isomers differ notably in glass-transition $T_g$ and sub-$T_g$ temperatures, and hence in dynamic properties.[21,44] 6FDA−6FpDA displays a $T_g$ at 593 K and three secondary transitions, among which an intense one at 391.5 K. In the case of 6FDA−6FmDA, the $T_g$ is at 527 K, with a sub-$T_g$ transition at 422 K which is more difficult to distinguish as it appears as a shoulder to the $T_g$. While the $T_g$ of 6FDA−6FmDA is lower than that of 6FDA−6FpDA, there is an obvious change in the slope of $CO_2$ permeability *vs* $T$ at the sub-$T_g$ temperature of 391.5 K, which is only found in 6FDA−6FpDA. Sub-$T_g$ transitions are thus thought to be more indicative of the chain motions that are necessary for diffusion to occur in glassy polymers than $T_g$ and the subtle chain motions that begin near 391.5 K in the *para*-isomer are likely to be associated with enhanced gas transport. On the other hand, the lack of a similar high-intensity sub-$T_g$ transition in 6FDA−6FmDA is attributed to an increased intersegmental and intrasegmental steric resistance in the nonsymmetric *meta* unit. This restricted local mobility of *meta*-linked phenylene rings permits more efficient packing and, as a consequence, 6FDA−6FmDA is slightly more densely packed than 6FDA−6FpDA.[21,23,44,78] This is summarized by Coleman et al.,[21] who attribute the primary effect of isomerism on the relative resistance to chain motions with a secondary effect on chain packing. The dynamic relaxations described above are difficult to reproduce with molecular models where the extremely fast cooling−heating rates (typically of the order of 0.1−1 K $ps^{-1}$) are many orders of magnitude higher than those used in experiments. However, in terms of model free-volumes, the *meta*-connected isomer does tend to have a consistently slightly smaller probe-accessible volume than the *para*-connected isomer, whatever the probe radius used,[11] and thus the average cavity size in 6FDA−6FpDA should be larger than that in the 6FDA−6FmDA isomer,[79] even if we are not aware of any experiments, e.g., positron annihilation, which actually tried to determine this directly. Interestingly, the trend of the *meta*-connected polyimide having lower permeabilities than the *para*-connected ones is a general one.[80−82] In their comparison of gas permeabilities in fluorinated and nonfluorinated polyimides,[13] the 19 systems studied by Tanaka et al. included *meta*-linked PMDA−mp′ODA and *para*-linked PMDA−pp′ODA as well as *meta*-linked 6FDA−mp′ODA and *para*-linked 6FDA−pp′ODA. Although the diamine is not the same as the one studied here, the *meta*-linked systems consistently have a lower $T_g$, a slightly higher density and, thus, a lower fractional free volume. Although differences in densities are quite small (0.011 g $cm^{-3}$ between MDA−mp′ODA and PMDA−pp′ODA, and 0.006 g $cm^{-3}$ between 6FDA−mp′ODA and 6FDA−pp′ODA), the permeability for $CO_2$ is found to be ∼3 times larger in both *para* isomers compared to their *meta* counterparts. This ratio is mostly due to the

differences in diffusion coefficients which also differ by a factor of ~2−3. In the same vein, the 6FDA−ODA *para* isomer has been reported as having a $CO_2$ permeability which is twice that of the *meta* isomer by Stern et al.[83] while Matsumoto et al. report a difference of 3.8 for exactly the same polymers.[8,9] They also studied other *para*-*meta* pairs, which lead to differences in $P_{CO_2}$ of ~2.4 for 6FDA−TPE and of ~3.5 for 6FDA−BAPS.[8,9] In all cases, the *para*-connected polyimides exhibit a higher $T_g$, lower density, and a higher gas permeability than their *meta*-connected isomers. Our model results for 6FDA−6FpDA and 6FDA−6FmDA are clearly much closer to the typical experimental ratios between the permeabilities of *para*- and *meta*-connected structures than the factor of 12 reported by Coleman et al. for both isomers under study.[12] Interestingly, the same authors report that thermal hysteresis has a significant effect on $P_{CO_2}$ with a *para*- vs *meta*-difference falling to 8 when the samples have been quenched from 15 °C above $T_g$ into an ice bath, in spite of the fact that quenching only results in small variations in the respective FFV and densities.[78] It is clear that the measured coefficients are strongly dependent on the processing conditions. Our models thus display the typical *para*- vs *meta*- trend found elsewhere, but not up to the unusually high value given for the two isomers in the literature.

In 6FDA−DAM, the bulkiness of the methyl groups should make chain packing less efficient. It has long been reported that a key factor in controlling the diffusion coefficient and selectivity for glassy polymers is the packing density associated with the local mobility of polymer chains. Tanaka et al. suggested that the high fraction of large holes created by packing irregularities when methyl substituents are added to the diamine motif are an important feature in the large increase of diffusivities associated with much lower $CO_2/CH_4$ selectivities.[14] In our MD simulations of the pure polymers,[11] the average fractional free volumes ($\langle FFV \rangle$) of the polymers were calculated using $\langle FFV \rangle = (\langle V \rangle - V_0)/\langle V \rangle$ with $\langle V \rangle$ being the average volume of the simulation box and $V_0$ the volume at 0 K (i.e., 1.3 times the van der Waals volume).[84] The $\langle FFV \rangle$ value of ~0.180 obtained for 6FDA−DAM was indeed higher than that of 6FDA−6FpDA (~0.175) and 6FDA−6FmDA (~0.167). However, the void space analyses suggest that the slightly larger amount of void volume in 6FDA−DAM is associated with a larger number of smaller cavities rather than to bigger cavities with respect to the two isomers.[11] This is not unexpected if one considers the steric effect of the methyl substituent on the diamine motif. The packing density of each polymer, i.e., the ratio between the mass of the polymer and the actual volume of the simulation box, is displayed in Figure 9 as a function of the nominal $CO_2$ concentration.

The packing densities present the sorption−desorption hysteresis behavior of the volume in a different way. Higher $D_{CO_2}$ are clearly correlated to lower matrix packing densities in these polyimides (see Figure 8). While the differences between 6FDA−6FpDA and 6FDA−6FmDA remain fairly small, in agreement with their pure densities, the 6FDA−DAM matrix is significantly less dense during desorption (Figure 9). This should favor diffusivity for penetrants such as $CO_2$ which do not seem to have preferential interactions with specific groups on the polymer chain (Figure 5). However, the 6FDA−DAM and 6FDA−6FpDA model $D_{CO_2}$ during the sorption phase differ by less than a factor of 2 (Figure 8, parts a and c), so the differences in the pure polymer densities (~200 kg $m^{-3}$) do not lead on the MD time scale to the increase of 3−5 expected from their respective experimental $D_{CO_2}$.[10,12,14,18,21] This is due in part to the faster model $D_{CO_2}$ in 6FDA−6FpDA with respect to the experimental values and to the various experimental conditions, but it is also in agreement with the fact that the FFV of 0.180 in 6FDA−DAM is only marginally higher than the FFV of 0.175 for 6FDA−6FpDA. It is supported by experimental studies, which report FFV ranging between 0.177[85] and 0.190[86] for 6FDA−DAM and between 0.175[86] and 0.190[12] for 6FDA−6FpDA. In spite of its lower packing density, 6FDA−DAM has quite a low monomer length, 15.2 Å, with respect to 18.7 Å for 6FDA−6FpDA,[11] so that limits the amount of voids that can be created by the trimethyl substituents on the diamine. The most obvious difference between 6FDA−DAM and both isomers lies in the desorption curves (Figure 8 and Figure 9). While both isomers are quite similar, it is clear that the conditioning effect is much stronger in 6FDA−DAM.

To investigate whether the volume swelling has an influence on chain motion, the number-averaged MSDs of all polymer atoms at a time-interval $(t - t_0) = 4000$ ps have been calculated as a function of $CO_2$ concentration during loading and unloading. Although these MSDs are relatively small and subject to significant errors, they have been plotted in Figure 10 for both 6FDA−6FpDA and 6FDA−DAM. For clarity, the 6FDA−DAM MSDs during desorption are omitted but they basically follow the same trend as for 6FDA−6FpDA. For comparison, the polymer packing density of 6FDA−6FpDA during sorption and desorption is also shown in Figure 10. Despite the noise in the MSDs data, there is a clear tendency for chain motions to increase at the higher $CO_2$ concentrations in response to the decreasing polymer packing density. There is also an indication of hysteresis in the polymer MSDs which correlates with the partial recovery of the packing density.

It has been shown experimentally for sulfonated polymers that the glass transition temperature, $T_g$, decreases as the amount of dissolved $CO_2$ increases by ~2−2.5 K for each $cm^3$ (STP) $cm^{-3}$ of $CO_2$ added.[87,88] The depression of the $T_g$ upon exposure to $CO_2$ is also found in a series of other glassy polymers.[22] The results shown in Figure 10 are qualitatively consistent with the experimental observation that polymer mobility is enhanced in the swollen systems. In a further preliminary investigation of this effect, five samples of 6FDA−6FpDA containing $CO_2$ percentages ranging from 5% to 25% were heated from 308 to 1308 K at a rate of 0.1K/ps under constant pressure conditions. Plots (not shown) of the torsional potential energy against temperature displayed curves with changes in slopes which could be objectively fitted to a combination of two linear functions. The temperature of such transitions in the torsional potential vs $T$ plots decreased from ~850 K to ~750 K when increasing the amount of $CO_2$ from 5% to 25%. In terms of the corresponding nominal concentrations at 308 K, this would imply a depression of the $T_g$ by ~0.7 K for each $cm^3$ (STP) $cm^{-3}$ of $CO_2$. Considering the extremely high rate of heating ($10^{11}$ K/s), and the associated broadening and displacement of the glass transition to higher temperatures, this result is reasonably coherent with experimental observations. However, a more detailed study is beyond the scope of the present paper. In addition, the pure 6FDA−6FpDA model displayed a $T_g$ of ~700 K when being cooled down from the melt at the same rate (rather than being heated up from its glassy state), thus showing that results will clearly be dependent on the simulation conditions, in the same way than experimental results are dependent on the preparation and measurement conditions.

Swelling thus leads to a decrease in the intersegmental steric resistance to motion for the polymer,[23] but according to our models, this is mostly associated with very local

motions in the matrix. The hysteresis between sorption and desorption (filled and open circles in Figure 10) is clear to see but this amounts to fairly little increased mobility in terms of MSDs. No large-scale polymer relaxations are necessary to explain dilation and enhanced transport on the nanosecond time scale of these MD simulations. However it should be again stressed that while long-term effects are not captured, they may still be necessary for an accurate description of the phenomena observed in experiments.

The slower relaxations in 6FDA−DAM that lead to the greater hysteresis of the volume and $CO_2$ diffusion evident in Figure 8c are difficult to detect in the magnitudes of the polymer MSDs. These could be linked to the greater steric hindrance to chain motion that the methyl groups provide and are presumably the reason for the higher $T_g$ of 6FDA−DAM, but direct evidence of this probably requires more subtle analyses. It should also be noted that, in spite of the high loadings, the packing density remains over 1100 kg m$^{-3}$ (Figure 9), i.e., it is still quite high. The differences in packing densities between the pure polymer systems and their highest loadings are found to be 200−230 kg m$^{-3}$ for all three polyimides, *i.e.* about 15% of their respective pure polymer densities (Figure 9). This is consistent with a limited increase in polymer mobility.

Another point to reflect upon is that the penetrant diffusion coefficient is sometimes interpreted in the literature[18,23,24] within the framework of the "dual-mode" sorption (DMS) and the partial immobilization model[89−91] as originating from two separate diffusion coefficients: $D_D$ which would be associated with the penetrants dissolved in the amorphous densely packed region of the matrix and $D_H$ which would be associated with the penetrants residing in low-energy packing defects of glassy polymers. As reported for $O_2$ sorption in polyimides,[92] the gas uptake vs pressure curves can indeed be well described by the DMS sorption model (although its adjustable parameters are not constant but vary systematically with the pressure range used, which is clearly rather unsatisfactory),[90] but without any evidence of two different populations of sorbed species at the molecular level. Indeed, the individual trajectories systematically exhibit some combination of oscillations-in-voids and jumps (see section 3.1). This suggests that if there were two populations, each individual $CO_2$ molecule would contribute at time $t$ either to one or to the other depending on its position at that specific time. These observations undermine the two-populations basis of the DMS model, but it remains a popular way of fitting the data due to its simplicity. Within this context, it should be noted that in our MD simulations of $O_2$ sorption in ODPA−ODA polyimides[92] and $CO_2$ solubility in the 6FDA-based matrices under study here,[27] the Boltzmann weighted insertion energy probability density distributions were found to be Gaussian and consequently to support rather the one-population site-distribution (SD) model introduced by Kirchheim.[93,94]

**3.3. Temperature Dependence of $D_{CO_2}$.** As temperature increases, the mechanism of penetrant motion is expected to gradually change from the successions of oscillations within voids and jumping events to a more homogeneous liquid-like diffusion process.[53,95] However, the temperature dependence of the diffusion coefficient remains Arrhenius in nature as long as the mechanism is still largely in the low-temperature hopping regime,[44] which happens even over the glass transition region in glassy polymers.[95] This is the case at 700 K, which lies above the experimental $T_g$ of all three polyimides (reported from various experimental studies as being in the range 575−605 K for 6FDA−6FpDA, 640−670 K for 6FDA−DAM, and ∼530 K for 6FDA−6FmDA),[11] as can be seen in Figure 11:

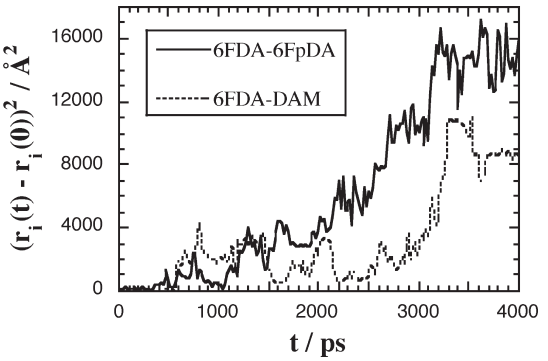


**Figure 11.** Individual displacements of $CO_2$ molecules belonging either to the 6FDA−6FpDA or to the 6FDA−DAM systems at 700 K, both being loaded with 3% $CO_2$.

If one compares Figure 3a at 308 K and Figure 11 at 700 K, it is clear that at higher temperatures, the jumps are more frequent and the time of residence in voids is much shorter. However, the basic mechanism still remains that of hopping-type rather than liquid-like diffusion. 700 K was the highest temperature considered for both 6FDA−6FmDA and 6FDA−DAM. 6FDA−6FpDA was actually studied over a larger (400−900 K) temperature range, but the trajectories at 900 K are qualitatively similar to those at 700 K. It is thus possible to write the Arrhenius equation for the diffusion coefficient as a function of temperature, $D(T)$ (eq 6):

$$D(T) = D_0 \exp\left(\frac{-E_d}{RT}\right) \tag{6}$$

Here $D_0$ is a prefactor, $E_d$ is the activation energy for diffusion, and $R$ is the gas constant. Additional simulations for all three polyimides under study were run at various temperatures $T$ ranging from 400 to 900 K and the corresponding diffusion coefficients $D(T)$ were directly extracted from the Fickian regime parts of the $CO_2$ MSDs vs time curves, identified by a slope of one in the log(MSD) − log(time) plots. Figure 12a shows the natural logarithm of $D(T)$ as a function of the reciprocal temperature for three different $CO_2$ loadings in the 6FDA−6FpDA polyimide. Fairly low loadings (1%, 3%, and 15%) were selected in order to account for the well-known decrease in solubility as temperature increases.[44] The actual simulation points are displayed with symbols only (filled and open circles, open squares) while the lines are the extrapolations of the MD results down to the experimental temperature range. The filled squares are the extrapolated model values at 308 K and the crosses are a series of experimental $CO_2$ diffusion coefficients at 308 K which can be found in the literature.[12,13,15,17,18,21] Please note that the experimental values are usually quoted for $CO_2$ pressures of 10 atm.

Figure 12a shows that the Arrhenius law holds very well for the 3% 6FDA−6FpDA system, where data were obtained more frequently at 100 K intervals. It was thus not considered necessary, in general, to obtain data at more than two well-separated temperatures. Extrapolations from different $CO_2$ loadings are reasonably consistent and lead to similar estimates of the diffusion coefficients at 308 K. These extrapolated values are found to be in good agreement with those obtained using TEKMC on the results at 308 K. The extrapolated $D_{CO_2}$ for 6FDA−6FpDA at 308 K using the Arrhenius approach is of the order of $\sim 2 \times 10^{-7}$ cm$^2$ s$^{-1}$, and that for 6FDA−DAM of $\sim 8 \times 10^{-7}$ cm$^2$ s$^{-1}$. Within the statistical resolution, they compare very well with the corresponding TEKMC values of $\sim 4.1 \times 10^{-7}$ cm$^2$ s$^{-1}$ for

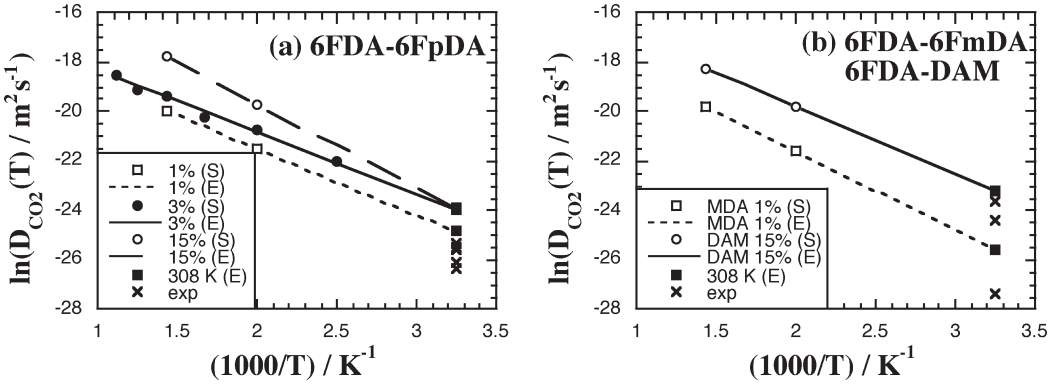


**Figure 12.** Logarithm of the $CO_2$ diffusion coefficient as a function of reciprocal temperature in (a) 6FDA−6FpDA loaded with 1%, 3%, and 15% $CO_2$ and (b) 6FDA−6FmDA loaded with 1% $CO_2$ and 6FDA−DAM loaded with 15% $CO_2$. The simulated data (S) obtained at $T \geq 400$ K are indicated by circles and open squares. The lines are extrapolations (E) of the simulated data, the filled squares are the extrapolated model values at 308 K and the crosses are experimental data available in the literature for the three polyimides under study.[12,13,15,17,18,21]

6FDA−6FpDA at 3% and $\sim 6.3 \times 10^{-7}$ cm$^2$ s$^{-1}$ for 6FDA−DAM at 15% as well as with the experimental values (Figure 12). The diffusion coefficient for 6FDA−6FmDA obtained from the Arrhenius approach is $\sim 0.8 \times 10^{-7}$ cm$^2$ s$^{-1}$, which is slightly lower than the TEKMC value of $1.8 \times 10^{-7}$ cm$^2$ s$^{-1}$ for 6FDA−6FmDA at 1%, but still larger than the experimental value of $\sim 0.134 \times 10^{-7}$ cm$^2$ s$^{-1}$ (lower cross in Figure 12b).[12] However, as noted before, there is often a scatter too in experimentally reported diffusion coefficients and the model ratio of ~2.5 between *para*- and *meta*- is quite consistent with other *para-vs-meta* studies. The high-temperature Arrhenius approach thus confirms both the results obtained for $D_{CO_2}$ using TEKMC at 308 K and the good agreement with experimental studies.

The activation energies for the diffusion $E_d$ can be obtained from the slopes of the plots displayed in Figure 12. $E_d$ is found to be approximately equal to ~6.6 kcal mol$^{-1}$ for 6FDA−6FpDA, ~6.3 kcal mol$^{-1}$ for 6FDA−6FmDA, and ~5.4 kcal mol$^{-1}$ for 6FDA−DAM. Although we are not aware of any experimental high-temperature data for the latter, Costello et al.[44] have measured gas permeabilities for several penetrants, among which $CO_2$, at temperatures up to 600 K for 6FDA−6FpDA and to 550 K for 6FDA−6FmDA. Gas solubilities were obtained at temperatures up to 473 K, and diffusion coefficients were obtained indirectly. In 6FDA−6FpDA, the activation energy for permeation $E_p$ is found to be consistently higher above the sub-$T_g$ temperature of 391.5 K than that below this temperature. The authors thus report two values for $E_p$, one below ~391.5 K and one above, attributing, as noted before, the difference to an enhanced segmental and vibrational motion above this secondary transition. The corresponding $E_d$ are 7.4 kcal mol$^{-1}$ above 391.5 K and 4.4 kcal mol$^{-1}$ below. Considering the differences in conditions and time scales between experiment and modeling, the model value of $E_d$ = 6.6 kcal mol$^{-1}$ for 6FDA−6FpDA obtained over a 400 K-900 K temperature range compares again rather favorably with the experimental value of 7.4 kcal mol$^{-1}$. There is an even better agreement for 6FDA−6FmDA with the model value of $E_d$ = 6.3 kcal mol$^{-1}$ falling very close to the experimental value of 6.6 kcal mol$^{-1}$.[44] The diffusion coefficients and activation energies of the model system are thus clearly validated by available experimental data.

## 4. Conclusion

$CO_2$ diffusivity in three glassy polyimides matrices has been studied up to contents of 30% (by mass) $CO_2$ by carrying out extensive fully atomistic MD simulations. To be consistent with the experimental approach and to avoid the necessity of artificially preswelling[26,41] the polyimide models, $CO_2$ loading was carried out progressively in increments of 2%. Conditioning was then assessed by removing $CO_2$ from the highest concentrations down in decrements of 2% in the same progressive way. This allowed us to cover the entire sorption and desorption model curves over a nominal $CO_2$ concentration range of 0−200 cm$^3$ (STP) cm$^{-3}$ for 6FDA−6FpDA, 6FDA−6FmDA, and 6FDA−DAM, which corresponded roughly to the 0−60 atm $CO_2$ pressure range.[27] The total number of MD simulations at 308 K was 84, each of them with a production run of 5000 ps, to which an additional 20 simulations (preliminary tests for $T_g$ and Arrhenius approach) were added in order to study the temperature dependence. Issues associated with solubility such as the $CO_2$ sorption and desorption isotherms, volume changes, void space characterization and energetic properties have already been addressed in a first paper.[27] In the present work, we analyzed the features associated with penetrant mobility and diffusion as a function of the polymer matrix, the $CO_2$ concentration and the sorption−desorption procedure.

In all cases, the behavior of $CO_2$ remains similar to that of smaller and less-soluble penetrants in glassy polymers,[45,46,48] i.e. the gas molecules oscillate within available free volumes in the polymer matrix and occasionally jump from one site to another through temporary channels related to the macromolecular fluctuations. It is interesting to note that, despite volume dilation in the higher loadings systems, there is no sign of transition from the hopping-type to the liquid-like regime. Radial distribution functions reveal that $CO_2$ is preferentially found in the vicinity of protruding chemical groups on the polymer, i.e., the carbonyl oxygens, fluorines and methyl hydrogens. It is less likely to come close to the more sheltered parts of the polymer and, unlike water,[55] it does not tend either to form any clusters inside the dense matrix.[27] A $CO_2$ penetrant is clearly quite free to access any part of the available free-volume in the polymer matrix providing, for purely space-occupying considerations, that such sites are not temporarily occupied by other penetrants.

Despite the fairly high intrinsic mobility of $CO_2$, the Fickian diffusive limit for the penetrant in the glassy polyimide matrices could not be reached over the 5000 ps time scale of our MD simulations. In order to estimate the limiting $CO_2$ diffusion coefficients $D_{CO_2}$ at 308 K, we introduced a variant of the kinetic Monte Carlo (KMC) approach, the "trajectory-extending kinetic Monte Carlo" (TEKMC) method. At the first stage, all the penetrant positions over the stored configurations were assigned to subcells of the primary MD box and a probability matrix for jumps to occur between specific subcells was constructed. At the

second stage, random walks were initiated from randomly selected subcells, and at each step of a walk, a subcell to jump to was selected with a probability corresponding to that found in the first phase. While the results were sensitive to the choice of the resolution of the subcell grid, this parameter could be easily tuned by first reproducing the MSDs over the time-interval of the original MD runs. TEKMC was found to be extremely efficient in these intermediate to high penetrant concentration systems at extending the penetrant trajectories (in the present state by more than 3 orders of magnitude, i.e., up to $10^7$ ps), and thus reaching the long-time Fickian diffusive limits. Its viability was confirmed by results obtained at higher temperatures, where the Fickian limit for diffusion could be reached directly within the time scale of the MD simulation. The $D_{CO_2}$ obtained using TEKMC at 308 K were also in agreement with an Arrhenius extrapolation of the higher temperature data to 308 K. We stress that the TEKMC approach is only valid in conditions where penetrant concentrations and mobilities are high enough to reveal a sufficient part of the available trajectories through the polymer system on the limited time scale of the MD simulations. As shown here for $CO_2$, this can be the case for relatively soluble penetrants at certain experimentally accessible pressure regimes. Further details of the TEKMC approach and its validation in the case of other small gas penetrants such as $O_2$, $N_2$, and $H_2O$ will be the subject of a separate article. However, more sophisticated techniques[46,48,62−67] are still required for obtaining diffusion coefficients of penetrants in the infinite dilution regime.

In all three models, volume dilation started above the nominal concentration range $C_0(CO_2) \approx 40-80$ cm$^3$ (STP) cm$^{-3}$, which includes the experimental $CO_2$ plasticization concentration for 6FDA−polyimides.[60,61] Following exposure to the highest $CO_2$ concentrations, the simulation box volumes decreased when $CO_2$ molecules were progressively removed, but did not recover the volumes found in the sorption phase. It is clear that both $CO_2$ plasticization and penetrant-induced hysteresis occur in glassy polymers over the few nanoseconds time scale available to MD simulation models, even if such models can only hope to capture the immediate effect of exposure to high $CO_2$ concentrations.

The $D_{CO_2}$ are found to be very closely linked to the volume swelling-contraction behavior and consequently to their respective polymer packing densities. They tend to remain fairly low and similar up to the start of plasticization. Since the lack of volume expansion at low concentrations has been correlated to the hole-filling mechanism,[27] this confirms that the mobility of one penetrant is unlikely to be affected by that of another penetrant, except for purely space-occupying considerations. The model $D_{CO_2}$ compare rather well with experimental values for both 6FDA−6FpDA and 6FDA−DAM, but they appear to be overestimated for 6FDA−6FmDA with respect to the only experimental value available.[12,21] On the other hand, the activation energies for diffusion obtained from the Arrhenius plots of the high-temperature data are validated by experimental data.[44] While model results and the small density difference between 6FDA−6FpDA and 6FDA−6FmDA cannot explain a $CO_2$ permeability ratio of 12 in favor of the *para* isomer, they do reproduce the general trend found for (*para*−*meta*) pairs,[80−82] i.e., differences on the order of 2−3 in favor of the *para* isomer. In 6FDA−DAM, the three methyl substituents on the DAM diamine motif lead to more inefficient chain packing. This favors diffusivity for $CO_2$, but the differences in FFV remain low because of the shorter monomer length of 6FDA−DAM with respect to both isomers.

As far as the higher $C_0$ are concerned, the increase in $D_{CO_2}$ is directly correlated to the gradual transition to an almost linear increase in volume at higher concentrations.[27] As expected, the hysteresis found in the volumetric analyses is also reflected in the diffusivities, with the $D_{CO_2}$ being quite a bit higher in desorption than in sorption. This hysteresis can be related to a fairly limited increase in polymer local mobility upon volume dilation, which means that the system is not able to relax sufficiently fast back to its initial structure upon desorption and thus lose the excess free-volume that has been created. The conditioning effect is stronger in the 6FDA−DAM system, which experimentally has the highest $T_g$ of the three polyimides studied.

This work has been carried out in bulk polymer models, which are periodic in three dimensions and do not carry any external surfaces. It would be interesting to address the effects of $CO_2$ sorption at the polymer interfaces. Studying volume dilation kinetics during sorption as has been done by Wessling et al.[25,92] would require true membrane models with the gas initially placed outside, as we have done previously for oxygen sorption in the ODPA−ODA polyimide.[92] In spite of the fact that realistic molecular models of glassy polymer membranes with explicit interfaces are far from being trivial, such work is actually in progress.

**Acknowledgment.** This work was granted access to the HPC resources of CCRT/CINES/IDRIS under the allocations 2009-095053 and 2010-095053 made by GENCI (Grand Equipement National de Calcul Intensif), France. The MUST cluster at the University of Savoie (France) and the MPIP (Germany) are also acknowledged for their generous provision of computer time.

## References and Notes

(1) Paul, D. R. *Sep. Purif. Rev.* **1976**, *5*, 33–50.
(2) Lonsdale, H. K. *J. Membr. Sci.* **1982**, *10*, 81–181.
(3) Wijmans, J. G.; Baker, R. W. *J. Membr. Sci.* **1995**, *107*, 1–21.
(4) Koros, W. J.; Mahajan, R. *J. Membr. Sci.* **2000**, *175*, 181–196.
(5) Yampolskii, Y.; Pinnau, I.; Freeman, B. D., *Materials Science of Membranes*; John Wiley & Sons Ltd.: Chichester, U.K., 2006.
(6) Kim, T. H.; Koros, W. J.; Husk, G. R. *Sep. Sci. Technol.* **1988**, *23*, 1611–1626.
(7) Ghosh, M. K.; Mittal, K. L., *Polyimides: fundamentals and applications*; Marcel Dekker, Inc.: New York, 1996.
(8) Matsumoto, K.; Xu, P.; Nishikimi, T. *J. Membr. Sci.* **1993**, *81*, 15–22.
(9) Matsumoto, K.; Xu, P. *J. Membr. Sci.* **1993**, *81*, 23–30.
(10) Tanaka, K.; Kita, H.; Okamoto, K.-I. *J. Polym. Sci., Part B: Polym. Phys.* **1993**, *31*, 1127–1133.
(11) Pandiyan, S.; Brown, D.; Van der Vegt, N. F. A.; Neyertz, S. *J. Polym. Sci., Part B: Polym. Phys.* **2009**, *47*, 1166–1180.
(12) Coleman, M. R.; Koros, W. J. *J. Membr. Sci.* **1990**, *50*, 285–297.
(13) Tanaka, K.; Kita, H.; Okano, M.; Okamoto, K.-I. *Polymer* **1992**, *33*, 585–592.
(14) Tanaka, K.; Okano, M.; Toshino, H.; Kita, H.; Okamoto, K.-I. *J. Polym. Sci., Part B: Polym. Phys.* **1992**, *30*, 907–914.
(15) Mikawa, M.; Nagaoka, S.; Kawakami, H. *J. Membr. Sci.* **1999**, *163*, 167–176.
(16) Yeom, C. K.; Lee, J. M.; Hong, Y. T.; Choi, K. Y.; Kim, S. C. *J. Membr. Sci.* **2000**, *166*, 71–83.
(17) Tanaka, K.; Kawai, T.; Kita, H.; Okamoto, K.-I.; Ito, Y. *Macromolecules* **2000**, *33*, 5513–5517.
(18) Wang, R.; Cao, C.; Chung, T.-S. *J. Membr. Sci.* **2002**, *198*, 259–271.
(19) Wang, L.; Cao, Y.; Zhou, M.; Ding, X.; Liu, Q.; Yuan, Q. *Polym. Bull.* **2008**, *60*, 137–147.
(20) Liu, Y.; Pan, C.; Ding, M.; Xu, J. *Polym. Int.* **1999**, *48*, 832–836.
(21) Coleman, M. R.; Koros, W. J. *J. Polym. Sci., Part B: Polym. Phys.* **1994**, *32*, 1915–1926.
(22) Ismail, A. F.; Lorna, W. *Sep. Pur. Technol.* **2002**, *27*, 173–194.
(23) Coleman, M. R.; Koros, W. J. *Macromolecules* **1997**, *30*, 6899–6905.
(24) Coleman, M. R.; Koros, W. J. *Macromolecules* **1999**, *32*, 3106–3113.
(25) Visser, T.; Wessling, M. *Macromolecules* **2007**, *40*, 4992–5000.
(26) Hölck, O.; Siegert, M. R.; Heuchel, M.; Böhning, M. *Macromolecules* **2006**, *39*, 9590–9604.
(27) Pandiyan, S.; Brown, D.; Neyertz, S.; Van der Vegt, N. F. A. *Macromolecules* **2010**, *43*, 2605–2621.

(28) Brown, D. *The gmq User Manual Version 4: available at* http://www.lmops.univ-savoie.fr/brown/gmq.html, 2008.
(29) Clark, M.; Cramer, R. D., III; Van Opdenbosch, N. *J. Comput. Chem.* **1989**, *10*, 982–1012.
(30) Frisch, M. J.; Trucks, G. W.; Schlegel, H. B.; Scuseria, G. E.; Robb, M. A.; Cheeseman, J. R.; Montgomery, J. A.; Vreven, J., T. ; Kudin, K. N.; Burant, J. C.; Millam, J. M.; Iyengar, S. S.; Tomasi, J.; Barone, V.; Mennucci, B.; Cossi, M.; Scalmani, G.; Rega, N.; Petersson, G. A.; Nakatsuji, H.; Hada, M.; Ehara, M.; Toyota, K.; Fukuda, R.; Hasegawa, J.; Ishida, M.; Nakajima, T.; Honda, Y.; Kitao, O.; Nakai, H.; Klene, M.; Li, X.; Knox, J. E.; Hratchian, H. P.; Cross, J. B.; Bakken, V.; Adamo, C.; Jaramillo, J.; Gomperts, R.; Stratmann, R. E.; Yazyev, O.; Austin, A. J.; Cammi, R.; Pomelli, C.; Ochterski, J. W.; Ayala, P. Y.; Morokuma, K.; Voth, G. A.; Salvador, P.; Dannenberg, J. J.; Zakrzewski, V. G.; Dapprich, S.; Daniels, A. D.; Strain, M. C.; Farkas, O.; Malick, D. K.; Rabuck, A. D.; Raghavachari, K.; Foresman, J. B.; Ortiz, J. V.; Cui, Q.; Baboul, A. G.; Clifford, S.; Cioslowski, J.; Stefanov, B. B.; Liu, G.; Liashenko, A.; Piskorz, P.; Komaromi, I.; Martin, R. L.; Fox, D. J.; Keith, T.; Al-Laham, M. A.; Peng, C. Y.; Nanayakkara, A.; Challacombe, M. P.; Gill, M. W.; Johnson, B.; Chen, W.; Wong, M. W.; Gonzalez, C.; Pople, J. A. *Gaussian 03*; Gaussian Inc.: Wallingford CT, 2004.
(31) Hammonds, K. D.; Ryckaert, J.-P. *Comput. Phys. Commun.* **1991**, *62*, 336–351.
(32) Zhang, Z.; Duan, Z. *J. Chem. Phys.* **2005**, *122*, 214507.
(33) Ciccotti, G.; Ferrario, M.; Ryckaert, J. P. *Mol. Phys.* **1982**, *47*, 1253–1264.
(34) Allen, M. P.; Tildesley, D. J., *Computer Simulation of Liquids*; Clarendon Press: Oxford, England, 1987.
(35) Ewald, P. P. *Ann. Phys.* **1921**, *369*, 253–287.
(36) Smith, W. *Comput. Phys. Commun.* **1992**, *67*, 392.
(37) Fincham, D. *Mol. Simul.* **1994**, *13*, 1–19.
(38) Berendsen, H. J. C.; Postma, J. P. M.; Van Gunsteren, W. F.; DiNola, A.; Haak, J. R. *J. Chem. Phys.* **1984**, *81*, 3684–3690.
(39) Brown, D.; Clarke, J. H. R. *Comput. Phys. Commun.* **1991**, *62*, 360–369.
(40) Neyertz, S. *Soft Mater.* **2007**, *4*, 15–83.
(41) Hölck, O.; Heuchel, M.; Böhning, M.; Hofmann, D. *J. Polym. Sci., Part B: Polym. Phys.* **2007**, *46*, 59–71.
(42) Van der Vegt, N. F. A.; Briels, W. J.; Wessling, M.; Strathmann, H. *J. Chem. Phys.* **1999**, *110*, 11061–11069.
(43) Humphrey, W.; Dalke, A.; Schulten, K. *J. Mol. Graphics* **1996**, *14*, 33–38.
(44) Costello, L. M.; Koros, W. J. *J. Polym. Sci., Part B: Polym. Phys.* **1995**, *33*, 135–146.
(45) Müller-Plathe, F. *Acta Polym.* **1994**, *45*, 259–293.
(46) Gusev, A. A.; Müller-Plathe, F.; van Gunsteren, W. F.; Suter, U. W. *Adv. Polym. Sci.* **1994**, *116*, 207–247.
(47) Gusev, A. A.; Suter, U. W.; Moll, D. J. *Macromolecules* **1995**, *28*, 2582–2584.
(48) Greenfield, M. L.; Theodorou, D. N. *Macromolecules* **1998**, *31*, 7068–7090.
(49) Neyertz, S.; Brown, D. *Macromolecules* **2004**, *37*, 10109–10122.
(50) Neyertz, S. *Macromol. Theory Simul.* **2007**, *16*, 513–524.
(51) Neyertz, S.; Brown, D. *Macromolecules* **2008**, *41*, 2711–2721.
(52) Boyd, R. H.; Pant, P. V. K. *Macromolecules* **1991**, *24*, 4078–4083.
(53) Pant, P. V. K.; Boyd, R. H. *Macromolecules* **1993**, *26*, 679–686.
(54) Bos, A.; Pünt, I. G. M.; Wessling, M.; Strathmann, H. *J. Membr. Sci.* **1999**, *155*, 67–78.
(55) Marque, G.; Neyertz, S.; Verdu, J.; Prunier, V.; Brown, D. *Macromolecules* **2008**, *41*, 3349–3362.
(56) Wick, C. D.; Siepmann, J. I.; Theodorou, D. N. *J. Am. Chem. Soc.* **2005**, *127*, 12338–12342.
(57) Fried, J. R.; Hu, N. *Polymer* **2003**, *44*, 4363–4372.
(58) Müller-Plathe, F.; Rogers, S. C.; Van Gunsteren, W. F. *Chem. Phys. Lett.* **1992**, *199*, 237–243.
(59) Cuthbert, T. R.; Wagner, N. J.; Paulaitis, M. E.; Murgia, G.; D'Aguanno, B. *Macromolecules* **1999**, *32*, 5017–5028.
(60) Coleman, M. R. Ph.D. Thesis, University of Texas: Austin, TX, 1988.
(61) Bos, A. Ph.D. Thesis, University of Twente: Twente, The Netherlands, 1996.
(62) Gusev, A. A.; Arizzi, S.; Suter, U. W.; Moll, D. J. *J. Chem. Phys.* **1993**, *99*, 2221–2227.
(63) Gusev, A. A.; Suter, U. W. *J. Chem. Phys.* **1993**, *99*, 2228–2234.
(64) Greenfield, M. L.; Theodorou, D. N. *Mol. Sim.* **1997**, *19*, 329–361.
(65) Greenfield, M. L.; Theodorou, D. N. *Macromolecules* **2001**, *34*, 8541–8553.
(66) Karayiannis, N. C.; Mavrantzas, V. G.; Theodorou, D. N. *Chem. Eng. Sci.* **2001**, *56*, 2789–2801.
(67) Karayiannis, N. C.; Mavrantzas, V. G.; Theodorou, D. N. *Macromolecules* **2004**, *37*, 2978–2995.
(68) Wessling, M.; Huisman, I.; Van der Boomgaard, T.; Smolders, C. A. *J. Polym. Sci., Part B: Polym. Phys.* **1995**, *33*, 1371–1384.
(69) Wessling, M.; Huisman, I.; Van der Boomgaard, T.; Smolders, C. A. *J. Appl. Polym. Sci.* **1995**, *58*, 1959–1966.
(70) Wind, J. D.; Sirard, S. M.; Paul, D. R.; Green, P. F.; Johnston, K. P.; Koros, W. J. *Macromolecules* **2003**, *36*, 6433–6441.
(71) Pandey, P.; Chauhan, R. S. *Prog. Polym. Sci.* **2001**, *26*, 853–893.
(72) Eastmond, G. C.; Page, P. C. B.; Paprotny, J.; Richards, R. E.; Shaunak, R. *Polymer* **1993**, *34*, 667–670.
(73) Mensitieri, G.; Del Nobile, M. A.; Monetta, T.; Nicodemo, L.; Bellucci, F. *J. Membr. Sci.* **1994**, *89*, 131–141.
(74) Joly, C.; Le Cerf, D.; Chappey, C.; Langevin, D.; Muller, G. *Sep. Purif. Technol.* **1999**, *16*, 47–54.
(75) Kawakami, H.; Mikawa, M.; Nagaoka, S. *J. Membr. Sci.* **1996**, *118*, 223–230.
(76) O'Brien, K. C.; Koros, W. J.; Husk, G. R. *Polym. Eng. Sci.* **1987**, *27*, 211–217.
(77) Kim, J. H.; Koros, W. J.; Paul, D. R. *J. Membr. Sci.* **2006**, *282*, 21–31.
(78) Fuhrman, C.; Nutt, M.; Vichtovonga, K.; Coleman, M. R. *J. Appl. Polym. Sci.* **2004**, *91*, 1174–1182.
(79) Wang, X.-Y.; In't Veld, P. J.; Lu, Y.; Freeman, B.; Sanchez, I. C. *Polymer* **2005**, *46*, 9155–9161.
(80) Robeson, L. M.; Smith, C. D.; Langsam, M. *J. Membr. Sci.* **1997**, *132*, 33–54.
(81) Alentiev, A. Y.; Loza, K. A.; Yampolskii, Y. P. *J. Membr. Sci.* **2000**, *167*, 91–106.
(82) Aitken, C. L.; Koros, W. J.; Paul, D. R. *Macromolecules* **1992**, *25*, 3424–3434.
(83) Stern, S. A.; Mi, Y.; Yamamoto, H. *J. Polym. Sci., Part B: Polym. Phys.* **1989**, *27*, 1887–1909.
(84) Van Krevelen, D. W., *Properties of polymers: their correlation with chemical structure; their numerical estimation and prediction from additive group contributions*, 3rd completely revised ed.; Elsevier: Amsterdam, 1990.
(85) Miyata, S.; Sato, S.; Nagai, K.; Nakagawa, T.; Kudo, K. *J. Appl. Polym. Sci.* **2007**, *107*, 3933–3944.
(86) Kim, J. H.; Koros, W. J.; Paul, D. R. *Polymer* **2006**, *47*, 3094–3103.
(87) Krause, B.; Sijbesma, H. J. P.; Münüklü, P.; Van der Vegt, N. F. A.; Wessling, M. *Macromolecules* **2001**, *34*, 8792–8801.
(88) Krause, B.; Mettinkhof, R.; Van der Vegt, N. F. A.; Wessling, M. *Macromolecules* **2001**, *34*, 874–884.
(89) Paul, D. R. *Ber. Bunsen-Ges.* **1979**, *83*, 294–302.
(90) Bondar, V. I.; Kamiya, Y.; Yampolskii, Y. P. *J. Polym. Sci., Part B: Polym. Phys.* **1996**, *34*, 369–378.
(91) Kanehashi, S.; Nagai, K. *J. Membr. Sci.* **2005**, *253*, 117–138.
(92) Neyertz, S.; Brown, D. *Macromolecules* **2009**, *42*, 8521–8533.
(93) Kirchheim, R. *Macromolecules* **1992**, *25*, 6952–6960.
(94) Gotthardt, P.; Grüger, A.; Brion, H. G.; Plaetschke, R.; Kirchheim, R. *Macromolecules* **1997**, *30*, 8058–8065.
(95) Bharadwaj, R. K.; Boyd, R. H. *Polymer* **1999**, *40*, 4229–4236.